Metabolic Activation of Benzodiazepines by CYP3A4 [S]

Katsuhiko Mizuno, Miki Katoh,[1] Hirotoshi Okumura, Nao Nakagawa, Toru Negishi,
Takanori Hashizume, Miki Nakajima, and Tsuyoshi Yokoi

Drug Metabolism and Toxicology, Faculty of Pharmaceutical Sciences, Kanazawa University, Kanazawa, Japan (K.M., M.K., H.O., N.N., M.N., T.Y.); and Pharmacokinetics Research Laboratories, Dainippon Sumitomo Pharma Co., Ltd., Osaka, Japan (T.N., T.H.)

ABSTRACT:

Cytochrome P450 3A4 is the predominant isoform in liver, and it metabolizes more than 50% of the clinical drugs commonly used. However, CYP3A4 is also responsible for metabolic activation of drugs, leading to liver injury. Benzodiazepines are widely used as hypnotics and sedatives for anxiety, but some of them induce liver injury in humans. To clarify whether benzodiazepines are metabolically activated, 14 benzodiazepines were investigated for their cytotoxic effects on HepG2 cells treated with recombinant CYP3A4. By exposure to 100 μM flunitrazepam, nimetazepam, or nitrazepam, the cell viability in the presence of CYP3A4 decreased more than 25% compared with that of the control. In contrast, in the case of other benzodiazepines, the changes in the cell viability between CYP3A4 and control Supersomes were less than 10%. These results suggested that nitrobenzodiazepines such as flunitrazepam, nimetazepam, and nitrazepam were metabolically activated by CYP3A4, which resulted in cytotoxicity. To identify the reactive metabolite, the glutathione adducts of flunitrazepam and nimetazepam were investigated by liquid chromatography-tandem mass spectrometry. The structural analysis for the glutathione adducts of flunitrazepam indicated that a nitrogen atom in the side chain of flunitrazepam was conjugated with the thiol of glutathione. Therefore, the presence of a nitro group in the side chain of benzodiazepines may play a crucial role in the metabolic activation by CYP3A4. The present study suggested that metabolic activation by CYP3A4 was one of the mechanisms of liver injury by nitrobenzodiazepines.

Drug-induced hepatotoxicity is one of the major causes of liver injury and is classified into intrinsic and idiosyncratic types. Intrinsic drug reactions can occur in a dose-dependent manner in any individual and are reproducible in preclinical studies. In contrast, idiosyncratic drug reactions do not occur in most patients at any dose, and they are often referred to as rare, with a typical incidence of from 1/100 to 1/100,000 (Uetrecht, 1999). Because idiosyncratic drug reactions are difficult to spot during drug development, some drugs launched on the market were later withdrawn because of idiosyncratic hepatotoxicity. Such drugs withdrawn for hepatotoxicity are known to produce reactive metabolites (Guengerich and MacDonald, 2007). The generation of reactive metabolites may relate to the formation of free radicals, oxidation of thiol, and covalent binding with endogenous macromolecules, resulting in the oxidation of cellular components or inhibition of normal cellular function (Guengerich and Liebler, 1985).

The generation of a reactive metabolite catalyzed by drug-metabolizing enzymes such as cytochrome P450 (P450) is defined as metabolic activation. P450 is the major drug-metabolizing enzyme that is highly expressed in human liver. CYP3A4 is the predominant isoform in liver (Shimada et al., 1994) and metabolizes more than 50% of the clinical drugs commonly used (Guengerich, 1995). However, CYP3A4 is also responsible for the formation of reactive metabolites of flutamide (Berson et al., 1993), trazodone (Kalgutkar et al., 2005), and troglitazone (Yamamoto et al., 2002). It is suggested that the reactive metabolites of flutamide, trazodone, and troglitazone cause the idiosyncratic hepatotoxicity in humans.

Prediction of the metabolic activation and the cytotoxicity of drug candidates is necessary in drug development. Human hepatocarcinoma HepG2 cells are commonly used for predicting hepatotoxicity in vitro. However, low expression levels of P450s in HepG2 cells may be responsible for the fact that 30% of the compounds were falsely classified as nontoxic (Rodriguez-Antona et al., 2002; Wilkening et al., 2003; Hewitt and Hewitt, 2004). In a recent study, a useful in vitro cell-based assay made by combining recombinant CYP3A4 with HepG2 cells was established (Vignati et al., 2005). It was demonstrated that hepatotoxicants whose reactive metabolites were generated by CYP3A4 exhibited cytotoxicity to the HepG2 cells. This assay system could be applied to screen for hepatotoxicity by drugs.
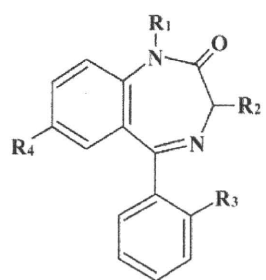
ABBREVIATIONS: P450, cytochrome P450; MTT, 3-(4,5-dimetylthiazol-2-yl)-2,5-diphenyl tetrazolium bromide; LC, liquid chromatography; MS/MS, tandem mass spectrometry; MS, mass spectrometry; LCMS-IT-TOF, liquid chromatography ion trap and time-of-flight mass spectrometry.

Benzodiazepine	R_1	R_2	R_3	R_4
Clonazepam	H	H	Cl	NO_2
Desmethyldiazepam	H	H	H	Cl
Diazepam	CH_3	H	H	Cl
Flunitrazepam	CH_3	H	F	NO_2
Flurazepam	$CH_2CH_2N(C_2H_5)$	H	F	Cl
Lorazepam	H	OH	Cl	Cl
Nimetazepam	CH_3	H	H	NO_2
Nitrazepam	H	H	H	NO_2
Norfludiazepam	H	H	F	Cl
Oxazepam	H	OH	H	Cl
Temazepam	CH_3	OH	H	Cl

Bromazepam

Chlordiazepoxide

Clobazam

FIG. 1. Chemical structures of the 14 benzodiazepines used in the present study.
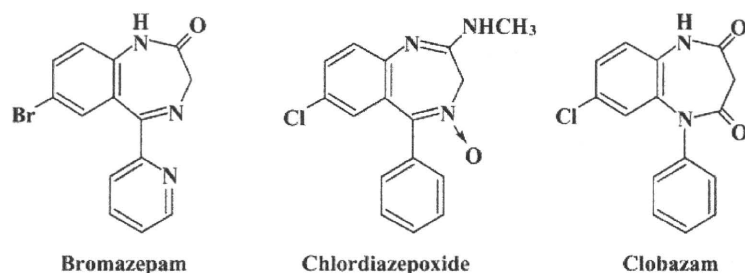
Benzodiazepines have been used extensively as hypnotics and sedatives for anxiety throughout the world. The mechanism of their efficacy is to amplify the action of γ-aminobutyric acid by acting as agonists at γ-aminobutyric acid receptors (Costa et al., 2002). Many benzodiazepines have been launched on the market and used in clinical practice. Two of the major benzodiazepines, flunitrazepam and nitrazepam, are widely used as hypnotic and anesthetic premedications in Europe and Japan. In 2001, it was announced by the Ministry of Health, Labor and Welfare of Japan that flunitrazepam induced hepatotoxicity. Chronic administration of antidepressant drugs including nitrazepam was reported to induce severe hepatic disorders (Seki et al., 2008). Clonazepam is one of the benzodiazepines used as an anxiolytic and anticonvulsant in clinical practice. Hepatic injury was reported to occur after treatment with clonazepam for 6 weeks in Ethiopia (Olsson and Zettergren, 1988).

The purpose of the present study was to clarify whether the metabolic activation of benzodiazepines by P450 occurs, leading to the hepatotoxicity. We investigated the cell viability in HepG2 cells in the presence or absence of CYP3A4 after exposure to 14 commercially available benzodiazepines (Fig. 1). There are many structural analogs of benzodiazepines, and the chemical structures and cytotoxicity in HepG2 cells were compared.

Materials and Methods

Materials. Clonazepam, clobazam, diazepam, lorazepam, nimetazepam, nitrazepam, and oxazepam were obtained from Wako Pure Chemicals (Osaka, Japan). Bromazepam, chlordiazepoxide, desmethyldiazepam, flunitrazepam, flurazepam, norfludiazepam, and temazepam were purchased from Sigma-Aldrich (St. Louis, MO). Human CYP2C9, 2C19, and 3A4 Supersomes (recombinant cDNA-expressed P450 enzymes prepared from a baculovirus insect cell system) and control Supersomes were purchased from BD Gentest (Woburn, MA). These microsomes coexpressed NADPH-cytochrome P450 reductase and cytochrome b_5. All other reagents used in this study were of the highest or analytical grade commercially available.

Cell Culture. Human hepatocarcinoma cell line HepG2 was obtained from Riken Gene Bank (Tsukuba, Japan). The cells were cultured in Dulbecco's modified Eagle's medium (Nissui Pharmaceutical, Tokyo, Japan) supple-

mented with 10% fetal bovine serum (Invitrogen, Melbourne, Australia) and 0.1 mM nonessential amino acids (Invitrogen) at 37°C in an atmosphere of 5% CO_2 and 95% air.

Cell Viability Assay. HepG2 cells were seeded at a density of 1×10^4 cells/well in 96-well plates with medium containing 3% fetal bovine serum, benzodiazepines, 8 nM human CYP2C9, CYP2C19, CYP3A4, or control Supersomes and 1 mM NADPH and then incubated at 37°C for 24 h. In the preliminary study, we investigated the cell viability in HepG2 cells with various P450 concentrations and incubation time. The 8 nM P450 and 24-h incubation were enough to detect cytotoxicity in this assay system. The final concentration of organic solvent (dimethyl sulfoxide) in medium was less than 0.2%. Cell viability after a 24-h incubation was evaluated by the intracellular ATP concentration using a CellTiter-Glo Luminescent Cell Viability Assay (ATP assay; Promega, Madison, WI) and 3-(4,5-dimetylthiazol-2-yl)-2,5-diphenyl tetrazolium bromide (MTT) activities using a CellTiter-Blue Cell Viability Assay (MTT assay; Promega). According to the protocols of the manufacturer, the luminescence of the generated oxyluciferin was measured in the ATP assay and the fluorescence of the generated resorufin was detected fluorometrically (excitation: 338 nm, emission: 458 nm) in the MTT assay by using a 1420 ARVO MX luminometer (PerkinElmer Wallac, Turku, Finland).

Caspase Assay. HepG2 cells were seeded under the same conditions and incubated at 37°C for 24 h. After incubation, the caspase 3/7 activity was measured using a Caspase-Glo 3/7 Assay (Promega) according to the protocol of the manufacturer. The luminescence of the generated aminoluciferin was measured using a 1420 ARVO MX luminometer.

Detection of Glutathione Adducts. A typical reaction mixture (final volume of 0.25 ml) contained 50 nM human CYP3A4 Supersomes, 100 mM potassium phosphate buffer (pH 7.4), an NADPH-generating system consisting of 0.775 mM nicotinamide adenine dinucleotide phosphate (oxidized form), 0.165 mM glucose 6-phosphate, 0.165 mM $MgCl_2$, 0.2 unit/ml glucose-6-phosphate dehydrogenase, 10 mM glutathione (reduced form), and 100 μM benzodiazepines (flunitrazepam, nimetazepam, nitrazepam, bromazepam, or temazepam). The final concentration of dimethyl sulfoxide in the reaction mixture was less than 1%. Incubation was performed at 37°C for 60 min and terminated by adding 0.75 ml of ice-cold methanol. After centrifugation at $15,000g$, the supernatant was subjected to liquid chromatography-tandem mass spectrometry (LC-MS/MS) (API 4000; Applied Biosystems, Foster City, CA). An LC-10 liquid chromatograph (Shimadzu, Kyoto, Japan) was used with an Inertsil ODS-3 analytical column (2.1 × 100 mm, 3 μm; GL Science, Tokyo, Japan). The column temperature was 40°C. The mobile phase was 10 mM ammonium acetate buffer (pH 4.0) (A) and acetonitrile (B). The conditions for

elution were as follows: 5 to 90% B (0–6 min), 90% B (6–11 min), 90 to 5% B (11–11.01 min), and 5% B (11.01–15 min). Linear gradients were used for all solvent changes. The flow rate was 0.2 ml/min. The liquid chromatograph was connected to an API 4000 mass spectrometer operated in the negative electrospray ionization mode. The turbo gas was maintained at 450°C. Air was used as the nebulizing and turbo gas at 60 psi. Nitrogen was used as the curtain gas at 20 psi. The collision energy was -50 V. The m/z 300 to 850 was scanned at the precursor ion (m/z 272; major mass spectrum fragment of glutathione).

Identification of Glutathione Adducts. Liquid chromatography ion trap and time-of-flight mass spectrometry (LCMS-IT-TOF) (Shimadzu) was used to identify the structures of the glutathione adducts of the nitrobenzodiazepines. The incubation mixture was the same as that described above except for CYP3A4 Supersomes (100 nM). Flunitrazepam and nimetazepam were used as test compounds. After centrifugation at $15,000g$ for 5 min, the supernatant was subjected to LCMS-IT-TOF using an Inertsil ODS-3 analytical column (2.1 × 100 mm, 3 μm). The LC conditions were the same as described earlier. The turbo gas was maintained at 450°C. Air was used as the nebulizing and turbo gas at 60 psi. Nitrogen was used as the curtain gas at 20 psi. The collision energy was 50 V. Structure analysis of the glutathione adducts of flunitrazepam and nimetazepam was performed by scanning at the product ion (m/z 621 and m/z 603, respectively) in the positive electrospray ionization mode.

Statistics. Data are expressed as mean $\pm$ S.D. ($n = 3$). Two groups were compared with a two-tailed Student's t test. $P < 0.05$ was considered statistically significant.

Results

Cell Viability of HepG2 Cells Treated with CYP3A4 and Benzodiazepines. HepG2 cells were incubated for 24 h with the 14 benzodiazepines at 50, 100, 200, and 400 μM in the presence of CYP3A4 or control Supersomes and then the cell viability was measured by the ATP and MTT assays. With exposure to 100 μM flunitrazepam, nimetazepam, and nitrazepam, cell viability in the presence of CYP3A4 Supersomes decreased more than 25% than with control Supersomes (Fig. 2). Although clonazepam could be dissolved up to 100 μM in the reaction mixtures, the viability of HepG2 cells treated with CYP3A4 Supersomes and 100 μM clonazepam exhibited 57 and 35% decreases in the ATP and MTT assays, respectively, compared with viability with control Supersomes (Supplemental Fig. 2). Flunitrazepam, nimetazepam, nitrazepam, and clonazepam are nitrobenzodiazepines that have a nitro group at the 7-position (Fig. 1). In contrast, for the other 10 benzodiazepines (bromazepam, chlordiazepoxide, clobazam, desmethyldiazepam, diazepam, flurazepam, lorazepam, norfludiazepam, oxazepam, and temazepam) at 100 μM, the changes in cell viability between CYP3A4 and control Supersomes were less than 10% and much smaller than those for the nitrobenzodiazepines (Fig. 2 and Supplemental Fig. 1). Moreover, 25% effective concentrations (EC_{25}) of nitrobenzodiazepines were less than 100 μM, and EC_{25} values of all other benzodiazepines were more than 300 μM in the ATP assay (Supplemental Table 1). Desmethyldiazepam, diazepam, flurazepam, lorazepam, norfludiazepam, and oxazepam exhibited concentration-dependent cytotoxicity in HepG2 cells incubated both with and without CYP3A4 (Fig. 2 and Supplemental Fig. 1).

Cell Viability on HepG2 Cells Treated with CYP2Cs and Nitrobenzodiazepines. It has been reported that CYP2C9 and CYP2C19 are involved in the metabolism of flunitrazepam (Hesse et al., 2001; Kilicarslan et al., 2001). Therefore, we investigated whether CYP2C9 and CYP2C19 affect the cytotoxicity caused by nitrobenzodiazepines in HepG2 cells. As shown in Fig. 3, the differences in the cell viability between CYP2Cs and control Supersomes when exposed to 100 μM nitrobenzodiazepines were less than 10%.

Caspase 3/7 Activity in HepG2 Cells Treated with CYP3A4 and Nitrobenzodiazepines. As a key factor of apoptosis, the caspase 3/7

activity was measured in HepG2 cells treated with CYP3A4 and the nitrobenzodiazepines for 24 h. Flunitrazepam, nimetazepam, and nitrazepam significantly increased the caspase 3/7 activities in HepG2 cells in the presence of CYP3A4 Supersomes (Fig. 4, A–C). In contrast, bromazepam as the negative control had no effects on the caspase 3/7 activities both with and without CYP3A4 (Fig. 4D).

Detection of Glutathione Adducts of Benzodiazepines. The glutathione adducts of benzodiazepines were investigated by the negative ion mode of LC-MS/MS. The nitrobenzodiazepines (flunitrazepam, nimetazepam, and nitrazepam) and the negative controls (bromazepam and temazepam) were measured. As shown in Fig. 5, the glutathione adducts of flunitrazepam and nimetazepam were detected in the presence of CYP3A4 Supersomes by precursor ion scans at m/z 619 and m/z 601 ($[M - H]^-$), respectively. In contrast, there were no adducts of flunitrazepam and nimetazepam when they were used in the control Supersomes (data not shown). In nitrazepam, bromazepam, and temazepam, glutathione adducts were not detected in the presence and absence of CYP3A4.

Identification of Glutathione Adducts of Flunitrazepam and Nimetazepam. The structures of the glutathione adducts of flunitrazepam and nimetazepam were estimated by the positive ion mode of LCMS-IT-TOF. For of the glutathione adduct of flunitrazepam, the product ion mass spectrum of m/z 621 ($[M + H]^+$) gave fragment ions at m/z 284.1, m/z 348.1, and m/z 492.1. The molecule weight of the $[M + H]^+$ fragment ion (m/z 492.1) meant that it was produced by the molecule weight of the compound (491) and that of a hydrogen ion (H^+; 1). The possible structure of the glutathione adduct of flunitrazepam is shown in Fig. 6. A reactive metabolite of flunitrazepam, in which the nitro group might be metabolized into the amino group, was conjugated to the 7-substituent group by glutathione.

On the other hand, the $[M + H]^+$ ion of the glutathione adduct of nimetazepam (m/z 603) gave fragment ions at m/z 266.4 and m/z 474.2 (Supplemental Fig. 3). The fragment ions at m/z 266.4 and m/z 474.2 were $[M + H - 337]^+$ and $[M + H - 129]^+$, respectively, corresponding to the fragment ions at m/z 284.1 and m/z 492.1 obtained from the glutathione adduct of flunitrazepam (m/z 621).

Discussion

In the present study, 14 benzodiazepine analogs were investigated for cytotoxic effects resulting from metabolic activation by CYP3A4. The major metabolic pathways of diazepam are 3-hydroxylayion by CYP3A4 and N-desmethylation by CYP2C9 (Schwartz et al., 1965; Ono et al., 1996). Thus, desmethyldiazepam, temazepam, and oxazepam are metabolites of diazepam (Fig. 1). In addition, norfludiazepam and nitrazepam would be the metabolites of flurazepam and nimetazepam, respectively.

The cytotoxicity of flunitrazepam, nimetazepam, nitrazepam, and clonazepam was observed in the presence of CYP3A4 Supersomes in HepG2 cells (Fig. 2 and Supplemental Fig. 1), suggesting that these three drugs are metabolically activated by CYP3A4. Flunitrazepam, nimetazepam, nitrazepam, and clonazepam are classified as nitrobenzodiazepines that have a nitro group in the side chain. In contrast, the other 10 benzodiazepines exhibited less cytotoxicity than the nitrobenzodiazepines (Fig. 2 and Supplemental Fig. 1; Supplemental Table 1). In the present study, we first clarified that the presence of a nitro group in the side chain of benzodiazepines may play a crucial rule in the metabolic activation by CYP3A4. To prevent the cytotoxicity by reactive metabolites in the medium, the effects of 200 μM or 1 mM glutathione (reduced form) were measured in this cell viability assay as a preliminary experiment. The glutathione recovered 10% of cell viability in HepG2 cells treated with CYP3A4 and 100 μM flunitraz-
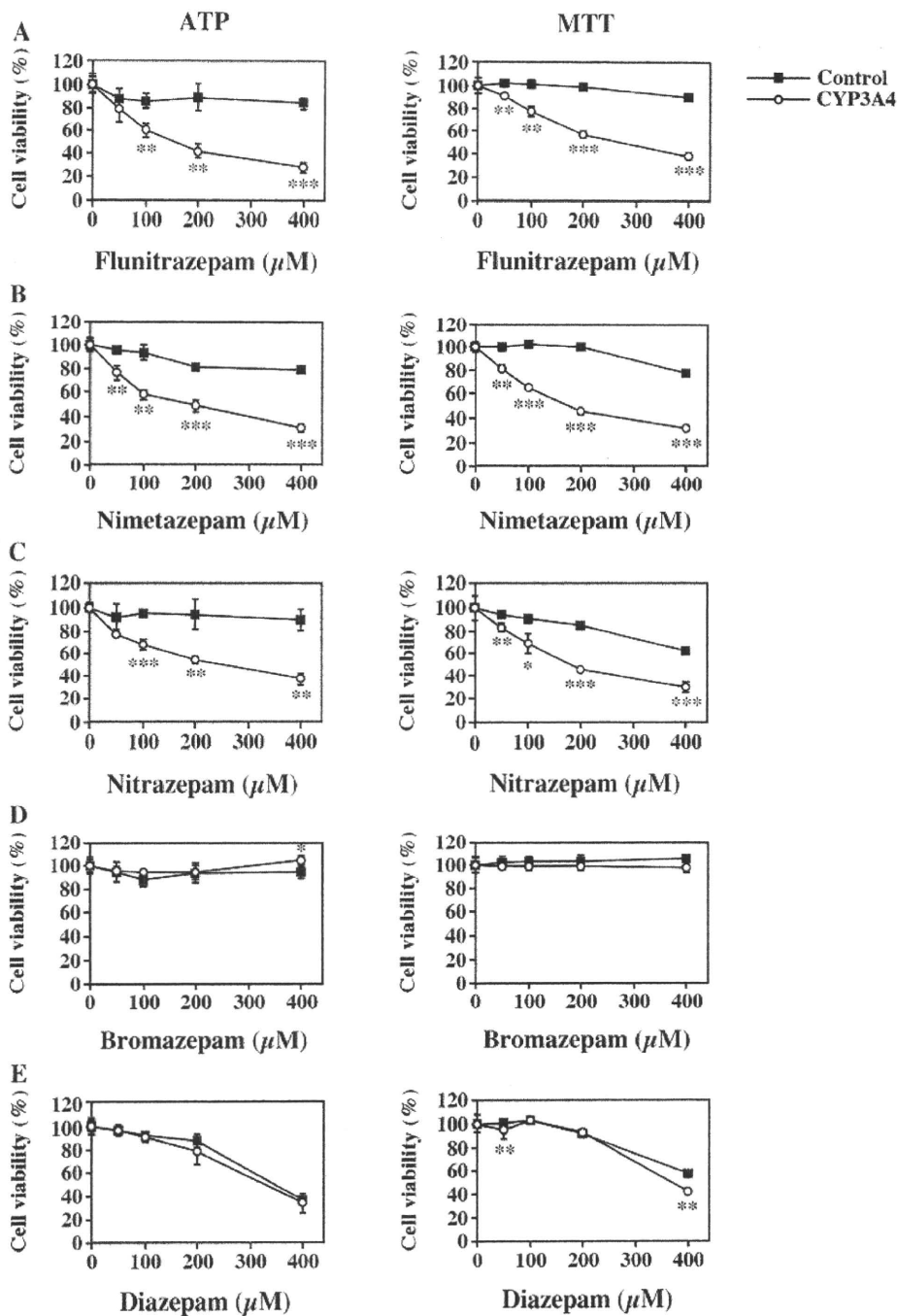
Fig. 2. Cytotoxicity of the benzodiazepines incubated with CYP3A4 on HepG2 cells. HepG2 cells seeded with the benzodiazepines and CYP3A4 or control Supersomes in 96-well plates were incubated at 37°C for 24 h. Cell viability was measured by ATP assay (left) and MTT assay (right) as described under *Materials and Methods*. The test compounds were flunitrazepam (A), nimetazepam (B), nitrazepam (C), bromazepam (D), and diazepam (E). Data represent the mean ± S.D. of three independent experiments. ∗, $P < 0.05$; ∗∗, $P < 0.01$; ∗∗∗, $P < 0.001$, compared with the control Supersomes.

epam (data not shown). This finding suggested that the reactive metabolites of nitrobenzodiazepines may bind to glutathione. However, glutathione did not completely protect against the cytotoxicity; thus, there may be another cytotoxic effect that could not be detoxified by glutathione trapping.

In humans, the major metabolites of flunitrazepam are *N*-desmethylflunitrazepam in plasma and 3-hydroxyflunitrazepam and 7-aminoflunitrazepam in urine (Fukazawa et al., 1978). CYP3A4 is the major P450 involved in flunitrazepam 3-hydroxylation and *N*-desmethylation, but CYP2C9 and CYP2C19 also catalyze the *N*-desmethylation of flunitrazepam (Hesse et al., 2001; Kilicarslan et al., 2001). The reductive metabolite of flunitrazepam, 7-aminoflunitrazepam, is cat-

alyzed by NADPH-cytochrome P450 reductase in HepG2 cells (Peng et al., 2004). Nimetazepam is metabolized to *N*-desmethylnimetazepam and 3-hydroxylnimetazepam (Dainippon Sumitomo Pharma, unpublished data). Nitrazepam is metabolized to 7-aminonitrazepam and 3-hydroxynitrazepam (Rieder, 1965). Although which P450 isoform mediates nimetazepam and nitrazepam metabolism has not been revealed, nimetazepam and nitrazepam may be metabolized by CYP2C9, CYP2C19, and CYP3A4. In our study, when HepG2 cells were exposed to 100 μM nitrobenzodiazepines, the differences in the cell viability between CYP2Cs and control Supersomes were less than 10% (Fig. 3), indicating that the contribution of CYP2Cs to the cytotoxicity of nitrobenzodiazepines was much lower than that of
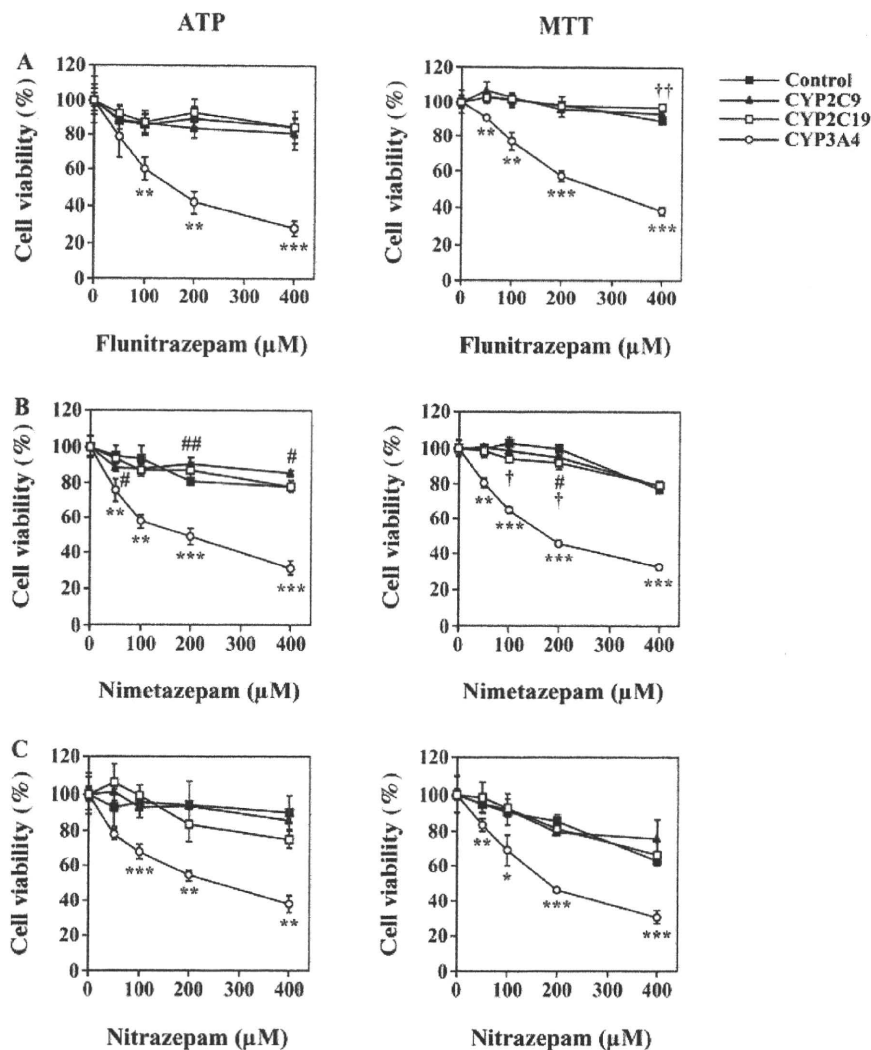
Fig. 3. Cytotoxicity of the benzodiazepines incubated with CYP2Cs in HepG2 cells. HepG2 cells seeded with the benzodiazepines and CYP2C9, CYP2C19, or control Supersomes in 96-well plates were incubated at 37°C for 24 h. Cell viability was measured by ATP assay (left) and MTT assay (right) as described under *Materials and Methods*. The test compounds were flunitrazepam (A), nimetazepam (B), and nitrazepam (C). Data for CYP3A4 and control Supersomes were redrawn from Fig. 2. Data represent the mean ± S.D. of three independent experiments. #, $P < 0.05$; ##, $P < 0.01$ (CYP2C9); †, $P < 0.05$; ††, $P < 0.01$ (CYP2C19); *, $P < 0.05$; **, $P < 0.01$; ***, $P < 0.001$ (CYP3A4), compared with the control Supersomes.

CYP3A4. Therefore, the metabolic activations of the nitrobenzodiazepines were CYP3A4-specific reactions.

Caspase 3 and 7 are classified as effector caspases. Active effector caspases mediate the cleavage of an overlapping set of protein substrates, resulting in the morphological features of apoptosis and the demise of the cell (Nuñez et al., 1998). Flunitrazepam, nimetazepam, and nitrazepam significantly increased the caspase 3/7 activities in HepG2 cells in the presence of CYP3A4 Supersomes (Fig. 4). Therefore, apoptosis after caspase 3 and 7 activation is one of the cytotoxic pathways of the reactive metabolites of flunitrazepam, nimetazepam, and nitrazepam.

The maximum plasma concentrations of nitrobenzodiazepines after a single administration in humans have been reported as follows: 0.04 μM after an oral dose of 2 mg of flunitrazepam (Fukazawa et al., 1978), 0.05 μM after an oral dose of 5 mg of nimetazepam (Dainippon Sumitomo Pharma, unpublished data), 0.3 μM after an oral dose of 10 mg of nitrazepam (Rieder, 1973), and 0.05 μM after an oral dose of 2 mg of clonazepam (Cavedal et al., 2007). Flunitrazepam was reported to induce hepatotoxicity by the Ministry of Health, Labor and Welfare of Japan, and nitrazepam and clonazepam were reported to cause drug-induced liver injury (Olsson and Zettergren, 1988; Seki et al., 2008). Although it is very difficult to extrapolate from an in vitro

study to in vivo in humans, we may pay attention to the metabolic activation of nitrobenzodiazepines by CYP3A4.

The metabolism of a nontoxic drug to reactive metabolites is thought to initiate a variety of adverse reactions (Park, 1986; Parke, 1987). Glutathione is an important intracellular peptide that can detoxify reactive metabolites by conjugation (Lu, 1999). Previous studies reported that reactive metabolites of flutamide (Kang et al., 2007), trazodone (Kalgutkar et al., 2005), and troglitazone (Kassahun et al., 2001) formed by CYP3A4 were detoxified by glutathione conjugations. As shown in Fig. 5, glutathione adducts of flunitrazepam and nimetazepam were detected by LC-MS/MS, suggesting the production of reactive metabolites of flunitrazepam and nimetazepam catalyzed by CYP3A4. In the present study, the structure of the glutathione adduct of flunitrazepam was estimated by LCMS-IT-TOF as shown in Fig. 6. It seemed that a nitrogen atom in the side chain of flunitrazepam was conjugated with the thiol of glutathione. The structure of the glutathione adduct of nimetazepam may be similar to that of flunitrazepam because the fragment ions, $[M + H - 337]^+$ and $[M + H - 129]^+$, corresponded to those of flunitrazepam (Supplemental Fig. 3). The glutathione adducts of nitrazepam could not be detected either with or without CYP3A4 in our detection system. However, the cytotoxicity of nitrazepam to HepG2 cells treated with CYP3A4
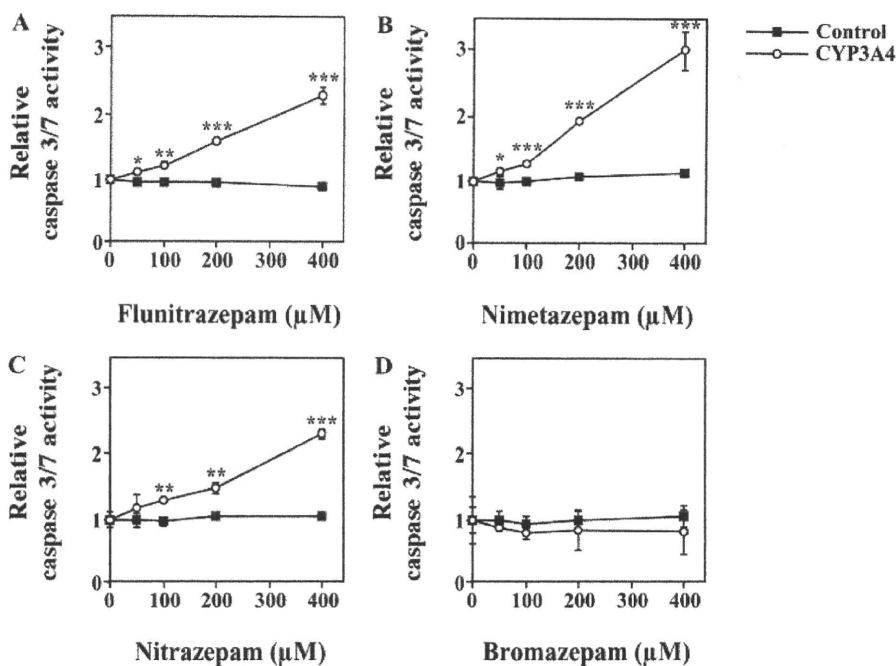
FIG. 4. Caspase 3/7 activity in HepG2 cells treated with CYP3A4 and the nitrobenzodiazepines. HepG2 cells in 96-well plates were incubated with benzodiazepines and CYP3A4 or control Supersomes at 37°C for 24 h. Caspase 3/7 activity was measured as described under *Materials and Methods*. The test compounds were flunitrazepam (A), nimetazepam (B), nitrazepam (C), and bromazepam (D). Data represent the mean ± S.D. of three independent experiments. *, $P < 0.05$; **, $P < 0.01$; ***, $P < 0.001$, compared with the control Supersomes.
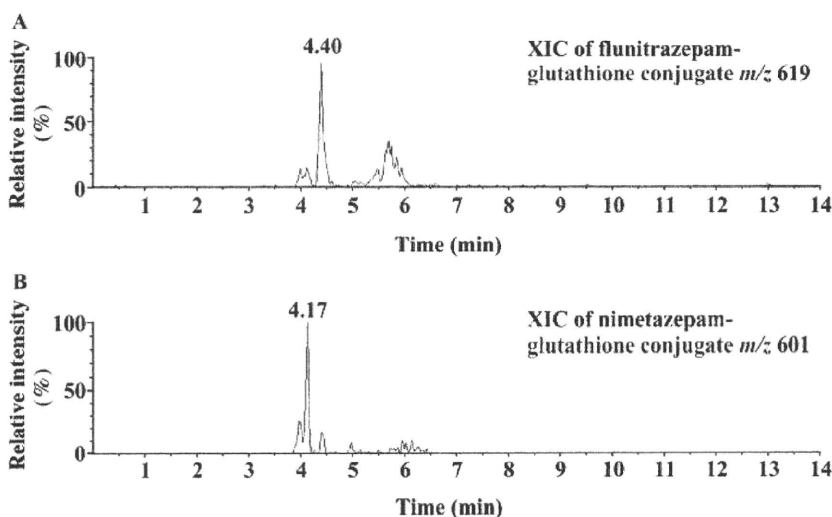

FIG. 5. Exacted ion chromatograms (XIC) of the glutathione adducts of benzodiazepines. The chromatograms were scanned with the precursor ion fragment, m/z 272, derived from glutathione using LC-MS/MS. A, flunitrazepam at m/z 619 ([M − H]$^-$); B, nimetazepam at m/z 601 ([M − H]$^-$).

Supersomes (Fig. 2) suggested that metabolic activation might occur. One of the reasons for this discrepancy may be the sensitivity of the detection.

Nitroaromatic drugs such as flutamide, nimesulide, and tolcapone have been associated with idiosyncratic liver injury (Boelsterli et al., 2006). In the reductive pathways from nitro to the fully reduced amine catalyzed by P450 and/or reductase, several reactive metabolites including nitroso and *N*-hydroxylamine derivatives could be produced. Such reactive metabolites seem to bind covalently to nucleophilic targets of proteins and nucleic acids, leading to the cytotoxic effects (Biaglow et al., 1986; Rickert, 1987; Kedderis and Miwa, 1988; Kedderis et al., 1989). On the other hand, arylamines are metabolically activated by P450-mediated *N*-hydroxylation. Electrophilic *N*-hydroxylamine reacts with intracellular molecules, which induce various types of toxicity including hepatotoxicity (Kato and Yamazoe, 1994). Flutamide induced severe hepatic dysfunction. Ohbuchi et al. (2008) suggested that CYP3A4 catalyzed the *N*-oxidation of the

amino metabolite of flutamide, which had hepatotoxic effects. Although the bioactivation pathways of nitrobenzodiazepines still remain unclear, they may undergo metabolic activation similar to that of other drugs. Further study is needed to clarify the mechanism of metabolic activation concerning nitrobenzodiazepines.

In conclusion, we revealed that nitrobenzodiazepines, such as flunitrazepam, nimetazepam, and nitrazepam, were metabolically activated by CYP3A4, resulting in cytotoxicity in HepG2 cells. The CYP3A4 metabolites of flunitrazepam and nimetazepam were conjugated with glutathione at a nitrogen atom in the side chain. This finding suggested that metabolic activation by CYP3A4 may be one of the mechanisms in liver injury. Moreover, we established a simple assay system in which the cytotoxicity in HepG2 cells incubated with recombinant P450s and the drug was observed with high sensitivity. This assay system was useful for detecting metabolic activation by P450s and would be beneficial for predicting drug-induced cytotoxicity in preclinical drug development.
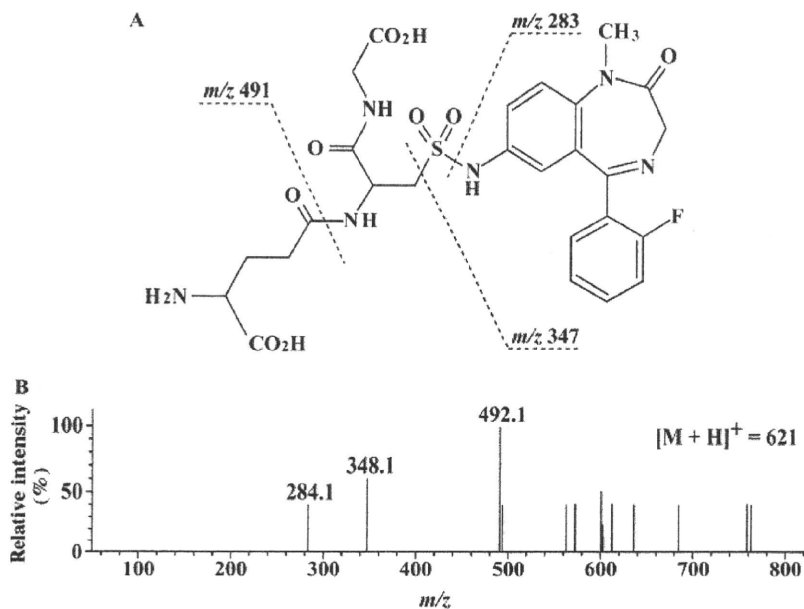
FIG. 6. A, predicted structure of the glutathione adduct of flunitrazepam. B, MS/MS spectra of the product ion obtained by collision-induced dissociation of the glutathione adduct of flunitrazepam at m/z 621 ([M + H]$^+$). These spectra were scanned using LCMS-IT-TOF.

References

Berson A, Wolf C, Chachaty C, Fisch C, Fau D, Eugene D, Loeper J, Gauthier JC, Beaune P, and Pompon D (1993) Metabolic activation of the nitroaromatic antiandrogen flutamide by rat and human cytochromes P-450, including forms belonging to the 3A and 1A subfamilies. *J Pharmacol Exp Ther* **265:**366–372.

Biaglow JE, Varnes ME, Roizen-Towle L, Clark EP, Epp ER, Astor MB, and Hall EJ (1986) Biochemistry of reduction of nitro heterocycles. *Biochem Pharmacol* **35:**77–90.

Boelsterli UA, Ho HK, Zhou S, and Leow KY (2006) Bioactivation and hepatotoxicity of nitroaromatic drugs. *Curr Drug Metab* **7:**715–727.

Cavedal LE, Mendes FD, Domingues CC, Patni AK, Monif T, Reyar S, Pereira Ados S, Mendes GD, and De Nucci G (2007) Clonazepam quantification in human plasma by high-performance liquid chromatography coupled with electrospray tandem mass spectrometry in a bioequivalence study. *J Mass Spectrom* **42:**81–88.

Costa E, Auta J, Grayson DR, Matsumoto K, Pappas GD, Zhang X, and Guidotti A (2002) GABA$_A$ receptors and benzodiazepines: a role for dendritic resident subunit mRNAs. *Neuropharmacology* **43:**925–937.

Fukazawa H, Ichishita H, Honda M, and Shimazu H (1978) Pharmacokinetics studies of flunitrazepam in healthy male Japanese subjects. *Jpn J Clin Pharmacol Ther* **9:**251–265.

Guengerich FP (1995) Human cytochrome P-450 enzymes, in *Cytochrome P-450* (Ortiz de Montellano PR eds) pp. 473–535, Premium, New York.

Guengerich FP and Liebler DC (1985) Enzymatic activation of chemicals to toxic metabolites. *Crit Rev Toxicol* **14:**259–307.

Guengerich FP and MacDonald JS (2007) Applying mechanisms of chemical toxicity to predict drug safety. *Chem Res Toxicol* **20:**344–369.

Hesse LM, Venkatakrishnan K, von Moltke LL, Shader RI, and Greenblatt DJ (2001) CYP3A4 is the major CYP isoform mediating the in vitro hydroxylation and demethylation of flunitrazepam. *Drug Metab Dispos* **29:**133–140.

Hewitt NJ and Hewitt P (2004) Phase I and II enzyme characterization of two sources of HepG2 cell lines. *Xenobiotica* **34:**243–256.

Kalgutkar AS, Henne KR, Lame ME, Vaz AD, Collin C, Soglia JR, Zhao SX, and Hop CE (2005) Metabolic activation of the nontricyclic antidepressant trazodone to electrophilic quinone-imine and epoxide intermediates in human liver microsomes and recombinant P4503A4. *Chem Biol Interact* **155:**10–20.

Kang P, Dalvie D, Smith E, Zhou S, and Deese A (2007) Identification of a novel glutathione conjugate of flutamide in incubations with human liver microsomes. *Drug Metab Dispos* **35:**1081–1088.

Kassahun K, Pearson PG, Tang W, McIntosh I, Leung K, Elmore C, Dean D, Wang R, Doss G, and Baillie TA (2001) Studies on the metabolism of troglitazone to reactive intermediates in vitro and in vivo. Evidence for novel biotransformation pathways involving quinone methide formation and thiazolidinedione ring scission. *Chem Res Toxicol* **14:**62–70.

Kato R and Yamazoe Y (1994) Metabolic activation of N-hydroxylated metabolites of carcinogenic and mutagenic arylamines and arylamides by esterification. *Drug Metab Rev* **26:**413–429.

Kedderis GL, Argenbright LS, and Miwa GT (1989) Covalent interaction of 5-nitroimidazoles with DNA and protein in vitro: mechanism of reductive activation. *Chem Res Toxicol* **2:**146–149.

Kedderis GL and Miwa GT (1988) The metabolic activation of nitroheterocyclic therapeutic agents. *Drug Metab Rev* **19:**33–62.

Kilicarslan T, Haining RL, Rettie AE, Busto U, Tyndale RF, and Sellers EM (2001) Flunitrazepam metabolism by cytochrome P450s 2C19 and 3A4. *Drug Metab Dispos* **29:**460–465.

Lu SC (1999) Regulation of hepatic glutathione synthesis: current concepts and controversies. *FASEB J* **13:**1169–1183.

Nuñez G, Benedict MA, Hu Y, and Inohara N (1998) Caspases: the proteases of the apoptotic pathway. *Oncogene* **17:**3237–3245.

Ohbuchi M, Miyata M, Nagai D, Shimada M, Yoshinari K, and Yamazoe Y (2008) Role of enzymatic N-hydroxylation and reduction in flutamide metabolite-induced liver toxicity. *Drug Metab Dispos* **37:**97–105.

Olsson R and Zettergren L (1988) Anticonvulsant-induced liver damage. *Am J Gastroenterol* **83:**576–577.

Ono S, Hatanaka T, Miyazawa S, Tsutsui M, Aoyama T, Gonzalez FJ, and Satoh T (1996) Human liver microsomal diazepam metabolism using cDNA-expressed cytochrome P450s: role of CYP2B6, 2C19 and 3A subfamily. *Xenobiotica* **26:**1155–1166.

Park BK (1986) Metabolic basis of adverse drug reaction. *J R Coll Phys Lond* **20:**195–200.

Parke DV (1987) Activation mechanisms to chemical toxicity. *Arch Toxicol* **60:**5–15.

Peng FC, Chaing HH, Tang SH, Chen PC, and Lu SC (2004) NADPH-cytochrome P-450 reductase is involved in flunitrazepam reductive metabolism in HepG2 and Hep3B cells. *J Toxicol Environ Health A* **67:**109–124.

Rickert DE (1987) Metabolism of nitroaromatic compounds. *Drug Metab Rev* **18:**23–53.

Rieder J (1965) Methods for estimating 1,3-dihydro-7-nitro-5-phenyl-2H-1,4-benzodiazepin-2-one and its principal metabolites in biological samples and results of research on the pharmacokinetics and metabolism of this compound in humans and rats. *Arzneimittel-Forschung* **15:**1134–1148.

Rieder J (1973) Plasma levels and derived pharmacokinetic characteristics of unchanged nitrazepam in man. *Arzneimittel-Forschung* **23:**212–218.

Rodríguez-Antona C, Donato MT, Boobis A, Edwards RJ, Watts PS, Castell JV, and Gómez-Lechón MJ (2002) Cytochrome P450 expression in human hepatocytes and hepatoma cell lines: molecular mechanisms that determine lower expression in cultured cells. *Xenobiotica* **32:**505–520.

Schwartz MA, Koechlin BA, Postma E, Palmer S, and Krol G (1965) Metabolism of diazepam in rat, dog, and man. *J Pharmacol Exp Ther* **149:**423–435.

Seki E, Taniguchi H, Nagano R, Sakitani Y, Serizawa T, Ito Y, Mine N, Mizuno H, Mitsuno Y, and Nakata R (2008) Case report: severe hepatic disorder induced by chronic administration of antidepressants drugs. *552nd Meeting for the Japanese Society of Internal Medicine Kanto Division*; 2008 Mar 8; Tokyo, Japan. 31 p, The Japanese Society of Internal Medicine, Tokyo.

Shimada T, Yamazaki H, Mimura M, Inui Y, and Guengerich FP (1994) Interindividual variations in human liver cytochrome P-450 enzymes involved in the oxidation of drugs, carcinogens and toxic chemicals: studies with liver microsomes of 30 Japanese and 30 Caucasians. *J Pharmacol Exp Ther* **270:**414–423.

Uetrecht JP (1999) New concepts in immunology relevant to idiosyncratic drug reactions: the "danger hypothesis" and innate immune system. *Chem Res Toxicol* **12:**387–395.

Vignati L, Turlizzi E, Monaci S, Grossi P, Kanter R, and Monshouwer M (2005) An in vitro approach to detect metabolite toxicity due to CYP3A4-dependent bioactivation of xenobiotics. *Toxicology* **216:**154–167.

Wilkening S, Stahl F, and Bader A (2003) Comparison of primary human hepatocytes and hepatoma cell line HepG2 with regard to their biotransformation properties. *Drug Metab Dispos* **31:**1035–1042.

Yamamoto Y, Yamazaki H, Ikeda T, Watanabe T, Iwabuchi H, Nakajima M, and Yokoi T (2002) Formation of a novel quinone epoxide metabolite of troglitazone with cytotoxicity to HepG2 cells. *Drug Metab Dispos* **30:**155–160.

Address correspondence to: Dr. Tsuyoshi Yokoi, Drug Metabolism and Toxicology, Faculty of Pharmaceutical Sciences, Kanazawa University, Kakuma-machi, Kanazawa 920-1192, Japan. E-mail: tyokoi@kenroku.kanazawa-u.ac.jp

Supplementary Fig. 1. Cytotoxicity of the benzodiazepines incubated with CYP3A4 on HepG2 cells. HepG2 cells seeded with the benzodiazepines and CYP3A4 or control Supersomes in 96-well plates were incubated at 37°C for 24 h. Cell viability was measured by ATP assay (left side) and MTT assay (right side) as described in *Material and Methods*. The test compounds were (A) chlordiazepoxide, (B) clobazam, (C) desmethyldiazepam, (D) flurazepam, (E) lorazepam, (F) norfludiazepam, (G) oxazepam, and (H) temazepam. Data represent the mean ± SD of three independent experiments. *$P < 0.05$; **$P < 0.01$; ***$P < 0.001$ compared with the control Supersomes.

ATP   MTT

E Lorazepam (μM)

F Norfludiazepam (μM)

G Oxazepam (μM)

**H** Temazepam (μM)
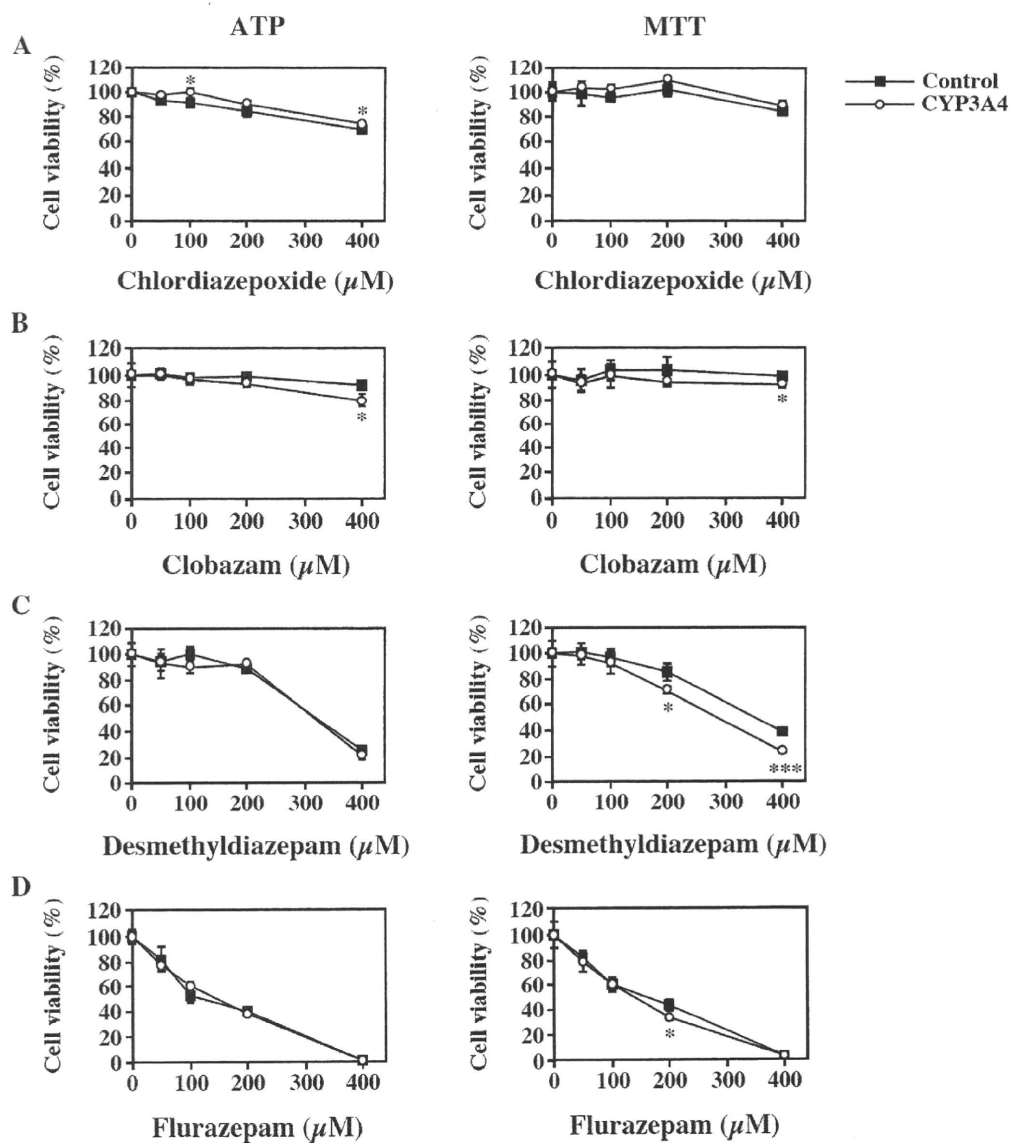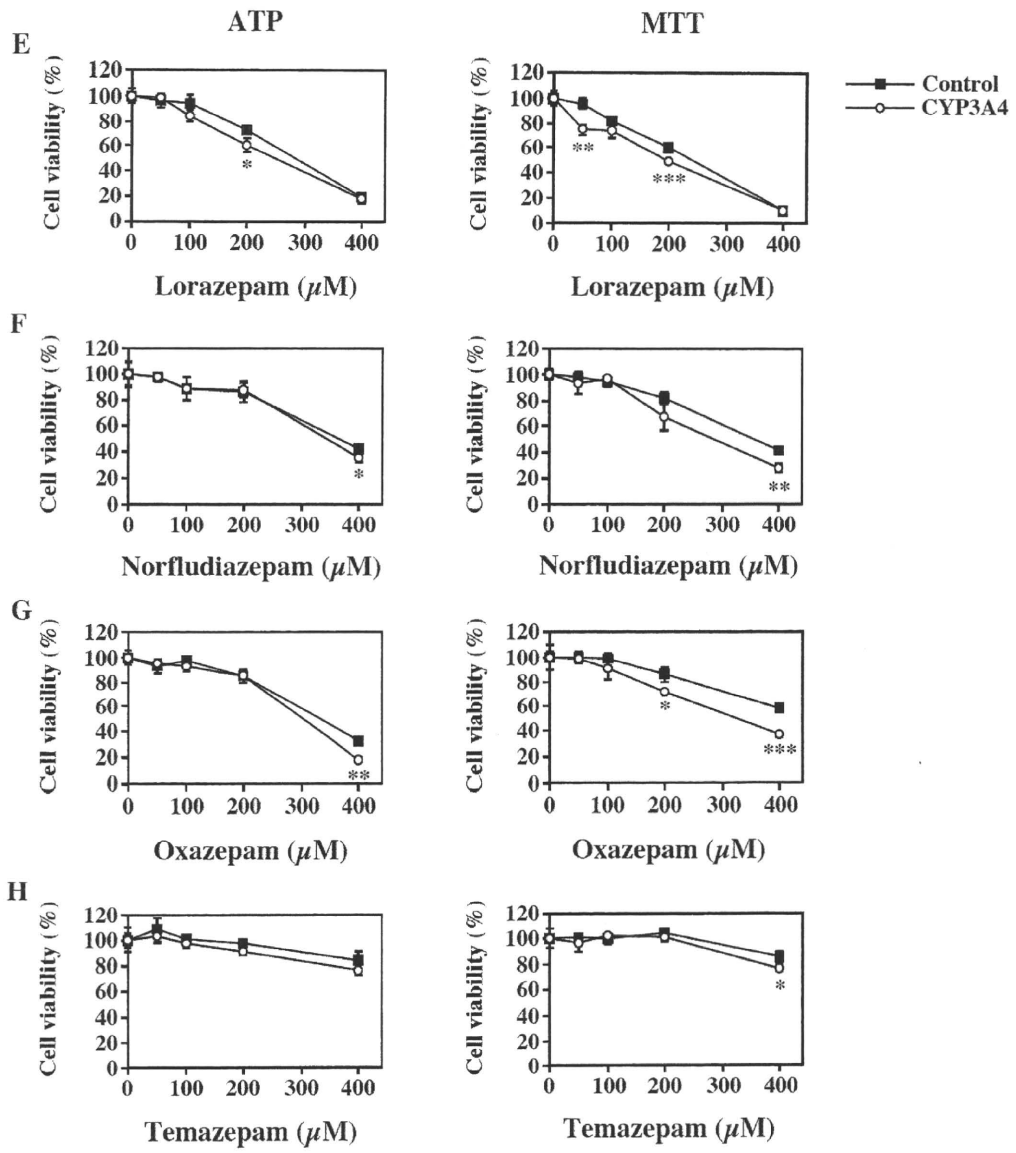
Control — CYP3A4

Supplementary Fig. 2. Cytotoxicity of clonazepam incubated with CYP3A4 in HepG2 cells.

HepG2 cells seeded with clonazepam and CYP3A4 or control Supersomes in 96-well plates were

incubated at 37°C for 24 h. Cell viability was measured by (A) ATP assay and (B) MTT assay as

described in *Material and Methods*. Data represent the mean ± SD of three independent experiments.

**P < 0.01; ***P < 0.001 compared with the control Supersomes.
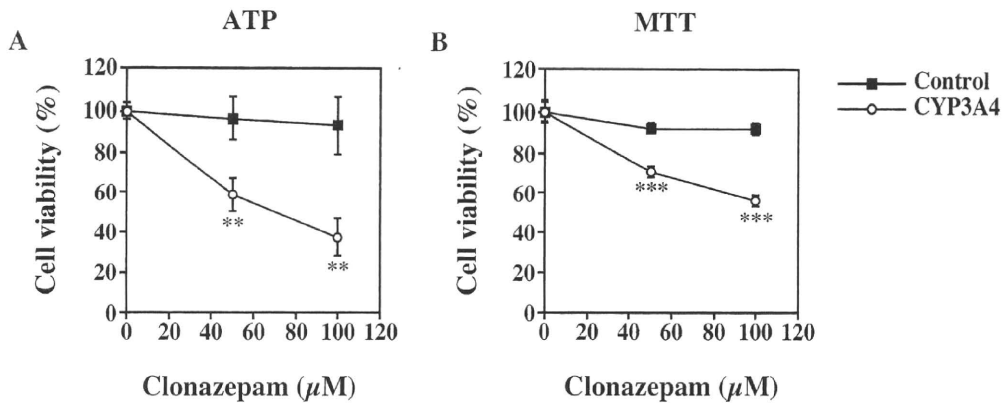
Supplementary Fig. 3. MS/MS spectra of product ion obtained by collision-induced dissociation of

the glutathione adduct of nimetazepam at *m/z* 603 ([M+H]$^+$). These spectra were scanned using

LCMS-IT-TOF. The collision energy was (A) 30 V and (B) 45 V, respectively.

239
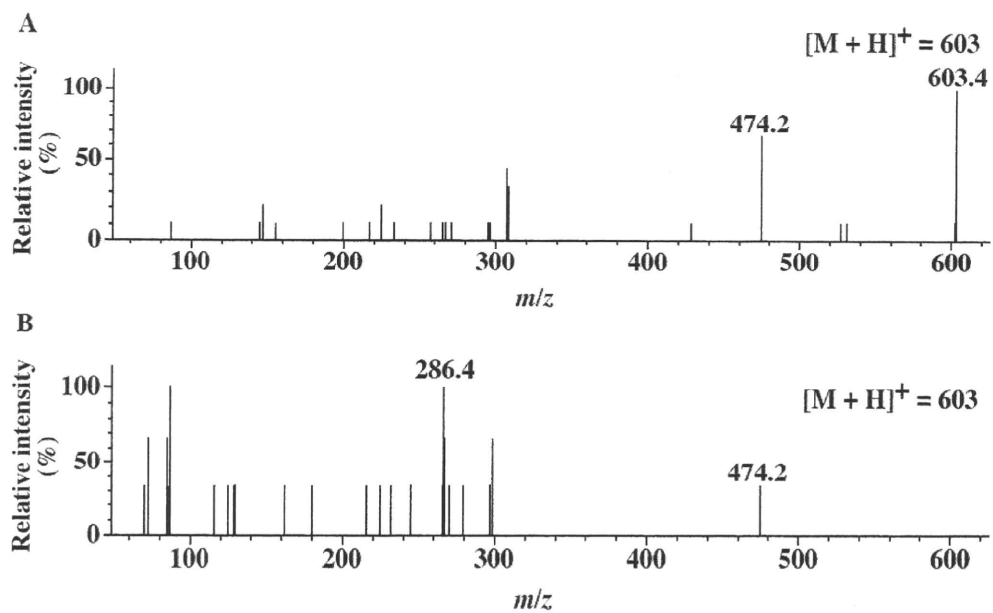
Supplementary Table 1. The 25% and 50% effective concentrations (EC$_{25}$ and EC$_{50}$) of

benzodizepines to HepG2 cells in ATP and MTT assays.

Benzodiazepine	ATP		MTT	
	EC$_{25}$(μM)	EC$_{50}$(μM)	EC$_{25}$(μM)	EC$_{50}$(μM)
Bromzepam	> 400	> 400	> 400	> 400
Chlordiazepoxide	> 400	> 400	> 400	> 400
Clobazam	> 400	> 400	> 400	> 400
Clonazepam	32.1	79.4	55.8	> 100
Desmethyldiazepam	> 400	> 400	270.8	> 400
Diazepam	> 400	> 400	384.8	> 400
Flunitrazepam	88.5	187.7	107.3	308.0
Flurazepam	> 400	> 400	> 400	> 400
Lorazepam	> 400	> 400	> 400	> 400
Nimetazepam	63.9	303.0	68.0	177.7
Nitrazepam	86.2	300.3	107.9	329.8
Norfludiazepam	> 400	> 400	304.7	> 400
Oxazepam	312.2	> 400	281.9	> 400
Temazepam	> 400	> 400	> 400	> 400

The EC$_{25}$ and EC$_{50}$ values were calculated by the rate of cell viability in HepG2 cells with CYP3A4

Supersomes divided by those in HepG2 cells incubated with the control Supersomes.

Different Inhibitory Effects in Rat and Human Carboxylesterases

Shiori Takahashi, Miki Katoh,[1] Takashi Saitoh, Miki Nakajima, and Tsuyoshi Yokoi

Drug Metabolism and Toxicology, Faculty of Pharmaceutical Sciences, Kanazawa University, Kanazawa, Japan

Received September 2, 2008; accepted February 12, 2009

ABSTRACT:

In vitro inhibition studies on drug-metabolizing enzyme activity are useful for understanding drug-drug interactions and for drug development. However, the profile of the inhibitory effects of carboxylesterase (CES) activity has not been fully investigated concerning species and tissue differences. In the present study, we measured the inhibitory effects of 15 drugs and 1 compound on CES activity using liver and jejunum microsomes and cytosol in human and rat. In addition, the inhibition constant (K_i values) and patterns were determined for the compounds exhibiting strong inhibition. Hydrolysis of imidapril and irinotecan hydrochloride (CPT-11) is catalyzed mainly by CES1 and CES2, respectively. In the inhibition study, imidaprilat formation from imidapril in human liver was strongly inhibited by nordihydroguaiaretic acid (NDGA) and procainamide. The inhibition profile and pattern were similar in human liver and rat liver. The compounds showing potent inhibition were similar between liver and jejunum. The K_i value of NDGA (K_i = 13.3 ± 1.5 μM) in human liver microsomes was 30-fold higher than that in rat liver microsomes (K_i = 0.4 ± 0.0 μM). On the other hand, 7-ethyl-10-hydroxycamptothecin (SN-38) formation from CPT-11 was not inhibited except by carvedilol, manidipine, and physostigmine. The K_i value of physostigmine (K_i = 0.3 ± 0.0 μM) in human jejunum cytosol was 10-fold lower than that in rat jejunum cytosol (K_i = 3.1 ± 0.4 μM) and was similar to that for manidipine. The present study clarified the species differences in CES inhibition. These results are useful for the development of prodrugs.

Carboxylesterase (CES) belongs to the α/β-hydrolase fold family and plays an important role in the hydrolysis of many esterified drugs such as anticancer and antihypertension drugs. There are species differences in CES isoforms between human and rat. In human, two major CES isoforms designated CES1 and CES2 have been characterized, and CES3 has recently been found in liver at considerably lower expression levels than those for the other CES isoforms (Sanghani et al., 2004). The mRNA expression levels of human CES1 are higher in liver than those in small intestine (Satoh et al., 2002), whereas human CES2 is abundant in small intestine (Schwer et al., 1997). On the other hand, in rat, there are several isoforms in CES1 and CES2 families. In the CES1 family, ES-10 (hydrolase A), ES-4 (hydrolase B/C), and ES-3 are mainly expressed in liver, and the mRNA expression levels of ES-10 are the highest of those of the three isoforms (Linke et al., 2005). ES-2 has been identified as CES (Murakami et al., 1993) and can hardly be detected in liver (Sanghani et al., 2002). Three rat CES2 mRNAs D50580, AB010635, and AY034877 have been found in various tissues such as liver, small intestine, stomach, and kidney (Sanghani et al., 2002).

The coadministration of drugs can affect their efficacy. Alterations in drug metabolism such as oxidation, reduction, and hydrolysis are often important causes of drug interactions. In particular, because

inhibition of drug-metabolizing enzymes is recognized as a prevalent factor, it is necessary to understand and clarify the inhibitory effects. The inhibitory effects of some compounds on CES activity have been previously reported for isomalathion (Buratti and Testai, 2005) and trifluoromethylketone-containing compounds (Wadkins et al., 2007). An anticancer drug, tamoxifen, has been found to be an inhibitor of human CES1 (Fleming et al., 2005) and rat ES-10 (Mésange et al., 2002). However, species differences in the inhibitory effects on CES activity have never been investigated comprehensively. In preclinical development of prodrugs catalyzed by esterases, information on differences in the inhibitory properties between rat and human is useful. In the present study, imidapril, an inhibitor of angiotensin-converting enzyme, and irinotecan hydrochloride (CPT-11) were used as typical substrates for CES1 and CES2, respectively (Takai et al., 1997; Humerickhouse et al., 2000; Sanghani et al., 2004). We investigated the species differences in the inhibitory effects of 15 drugs and 1 compound for two representative CES activities.

Materials and Methods

Materials. Imidapril hydrochloride and imidaprilat were kindly supplied by Mitsubishi Tanabe Pharma Corporation (Osaka, Japan). Delapril was kindly provided by Takeda Pharmaceutical Company (Osaka, Japan). Capecitabine was purchased from The United States Pharmacopeial Convention (Rockville, MD). Carvedilol was obtained from LKT Laboratories (St. Paul, MN). CPT-11, 7-ethyl-10-hydroxycamptothecin (SN-38), docetaxel trihydrate, temocapril hydrochloride, and temocaprilat were purchased from Toronto Research Chemicals (North York, ON, Canada). Acemetacin, dexamethasone, nordihydroguaiaretic acid (NDGA), procainamide hydrochloride, and proglumide were purchased from Sigma-Aldrich (St. Louis, MO). Camptothecin, cipro-

floxacin hydrochloride monohydrate, manidipine, nifedipine, and physostigmine sulfate were obtained from Wako Pure Chemicals (Osaka, Japan). Pooled human liver microsomes (HLM) and cytosol (HLC) were purchased from BD Gentest (Woburn, MA). Pooled human jejunum microsomes (HJM) and cytosol (HJC) were obtained from Tissue Transformation Technologies (Edison, NJ). All other chemicals and solvents were of analytical or the highest grade commercially available.

Preparation of Microsomes and Cytosol from Rat Liver or Jejunum. Male Wistar rats, 7 weeks old, were obtained from Japan SLC (Shizuoka, Japan). Pooled microsomes and cytosol from five rat livers (RLM and RLC) and jejunums (RJM and RJC) were prepared according to the method of Emoto et al. (2001).

Imidaprilat Formation. Imidaprilat formation from imidapril was determined according to the method of Takahashi et al. (2008) with slight modifications. A typical incubation mixture (200-μl total volume) contained the enzyme source, 100 mM Tris-HCl buffer (pH 7.4), and inhibitors. After a 2-min preincubation at 37°C, the reaction was initiated by the addition of imidapril, and then the mixture was incubated at 37°C for 30 min except for RLM and RLC (10 min). The reaction was terminated by adding 100 μl of ice-cold acetonitrile. After centrifugation at 9000g for 5 min, 10 μl of the supernatant was subjected to a liquid chromatography-tandem mass spectrometry system. The formed imidaprilat was quantified by the liquid chromatography-tandem mass spectrometry peak area of an authentic standard. The linearity of the standard curve of imidaprilat was confirmed ($r = 0.99$), and the imidaprilat in the incubation mixture was determined within the range. In the preliminary study, bis(p-nitrophenyl)phosphate, a CES specific inhibitor, (300 μM) inhibited the imidaprilat formation potently with all enzyme sources at 150 μM imidapril.

SN-38 Formation. SN-38 formation from CPT-11 was determined according to the method of Tabata et al. (2004) with slight modifications. A typical incubation mixture (200-μl total volume) contained the enzyme source, 100 mM potassium phosphate buffer (pH 7.4), and inhibitors. CPT-11 was dissolved in dimethyl sulfoxide (DMSO). The final concentration of DMSO in the reaction mixture was <1.0%. After a 2-min preincubation at 37°C, the reaction was initiated by the addition of CPT-11, and then the mixture was incubated at 37°C for 3 min except for RJM and RJC (2 min). The reaction was terminated by adding 200 μl of ice-cold acetonitrile, and 10 μl of 1 M HCl was then added. Camptothecin (20 pmol) was added as an internal standard. After centrifugation at 6500g for 5 min, 50 μl of the supernatant was subjected to high-performance liquid chromatography on an Inertsil ODS-3 analytical column (4.6 × 250 mm; GL Sciences, Inc., Tokyo, Japan). The eluent was fluorometrically monitored at an excitation of 380 nm and emission of 556 nm with a noise-base clean Uni-3 (Union, Gunma, Japan). The column temperature was 35°C, and the flow rate was 0.8 ml/min. The mobile phase consisted of 30% acetonitrile and 70% of 10 mM KH_2PO_4 containing 30 mM 1-heptanesulfonic acid sodium salt. The retention times of SN-38 and camptothecin were 13.3 and 16.3 min, respectively. The SN-38 formed was quantified by the high-performance liquid chromatography peak height of an authentic standard. The linearity of the standard curve of SN-38 was confirmed ($r = 0.99$), and the SN-38 in the incubation mixture was determined within the range. In the preliminary study, bis(p-nitrophenyl)phosphate (10 μM) inhibited the SN-38 formation potently with all enzyme sources at 5 μM CPT-11.

Inhibition Analysis of CES Activities. Inhibitory effects on imidaprilat and SN-38 formation were investigated using 15 drugs and 1 compound. Acemetacin, capecitabine, carvedilol, CPT-11, dexamethasone, docetaxel, manidipine, NDGA, nifedipine, temocapril, and temocaprilat were dissolved in DMSO. Ciprofloxacin, delapril, imidapril, physostigmine, procainamide, and proglumide were dissolved in distilled water. Capecitabine, delapril, and temocapril are CES substrates, whereas the other drugs and one compound are not. These compounds were added to the incubation mixtures described above to investigate their inhibitory effects on the imidaprilat and SN-38 formations. The final concentration of DMSO in the incubation mixture was <1% except for manidipine (2%) in the imidaprilat formation. All data were analyzed using the average of duplicate determinations.

For screening of the inhibitory effects, the imidaprilat formation at 150 μM imidapril was examined in the presence of 15 drugs and 1 compound (300 μM) except manidipine (50 μM). The SN-38 formation at 5 μM CPT-11 was determined in the presence of 15 drugs and 1 compound (10 μM).

For determination of the K_i (inhibition constant) values, the concentrations

of imidapril ranged from 100 to 500 μM for HLM and HLC, from 25 to 150 μM for RLM, from 15 to 90 μM for RLC, from 20 to 80 μM for RJM, and from 25 to 100 μM for RJC, respectively. The concentrations of the inhibitors ranged as follows: for carvedilol, 1 to 6 μM for RLM, 1 to 6 μM for RLC, 4 to 24 μM for RJM, and 5 to 30 μM for RJC; for NDGA, 10 to 40 μM for HLM, 2 to 7 μM for HLC, 0.2 to 2 μM for RLM, 0.2 to 1.5 μM for RLC, 3 to 15 μM for RJM, and 2 to 12 μM for RJC; and for procainamide, 25 to 150 μM for HLM and 25 to 100 μM for HLC. The protein concentrations of HLM, HLC, RLM, RLC, RJM, and RJC were 0.2, 1.0, 0.01, 0.05, 0.2, and 0.5 mg/ml, respectively. In the preliminary study, the rate of imidaprilat formation was linear with respect to all protein concentrations and incubation times.

For determination of the K_i values, the concentrations of CPT-11 ranged from 2.5 to 15 μM for all enzyme sources and the concentrations of inhibitors ranged as follows: for carvedilol, 2 to 8 μM for HLM and 1 to 12 μM for HLC; for manidipine, 0.1 to 0.5 μM for HJC, 0.5 to 5 μM for RJM, and 0.5 to 4 μM for RJC; and for physostigmine, 0.1 to 0.6 μM for HLM, 0.2 to 5 μM for HLC, 1 to 6 μM for HJM, 0.2 to 1 μM for HJC, 1 to 8 μM for RJM, and 2 to 10 μM for RJC. The protein concentrations of microsomes and cytosol were 0.2 and 1.0 mg/ml except for RJM and RJC (0.1 and 0.5 mg/ml), respectively. In the preliminary study, the rate of SN-38 formation was linear with respect to all protein concentrations and incubation times. The K_i values and inhibition types were determined by fitting the kinetic data to a competitive, noncompetitive, uncompetitive, or mixed inhibition model by nonlinear regression analysis using GraphPad Prism 5 (GraphPad Software Inc., San Diego, CA).

Results

Inhibitory Effects of 15 Drugs and 1 Compound on Imidaprilat Formation. The inhibitory effects on the imidaprilat formation were investigated using 15 drugs and 1 compound (Fig. 1). Imidaprilat formation in both HLM and HLC was moderately inhibited by acemetacin, carvedilol (only HLC), nifedipine, and procainamide (20–50% of control) and strongly inhibited by NDGA (<20% of control). On the other hand, all compounds except ciprofloxacin, dexamethasone (only RLC), and proglumide inhibited the imidaprilat formation by more than 50% in both RLM and RLC. In particular, delapril, temocapril, and temocaprilat, which are structurally similar to imidapril, showed stronger inhibitions in RLM and RLC than in HLM and HLC. The compounds exhibiting strong inhibition in RJM and RJC were similar to those in RLM and RLC. Imidaprilat formation in HJM and HJC was not detected at 200 μM imidapril; therefore, inhibition studies were not performed.

Inhibitory Effects of 15 Drugs and 1 Compound on SN-38 Formation. Fifteen drugs and one compound were screened for their inhibitory effects on SN-38 formation (Fig. 2). Screening of the inhibitory effects in HJM and HJC were performed only for six drugs and one compound because the lots of HJM and HJC available were limited. In both HLM and HLC, carvedilol, physostigmine, and manidipine (only HLC) inhibited SN-38 formation moderately (20–50% of control). In both RLM and RLC, SN-38 formation was not inhibited except by manidipine and NDGA, exhibiting weak inhibition (50–70% of control) only in RLC. These formations in both RJM and RJC were inhibited moderately by manidipine and physostigmine. SN-38 formation in HJC was inhibited moderately by carvedilol (20–50% of control) and inhibited strongly by manidipine and physostigmine, whereas this formation in HJM was inhibited strongly only by physostigmine.

Inhibition Constant and Inhibitory Patterns of Imidaprilat Formation. K_i values and inhibition patterns of the compounds showing strong inhibition for the imidaprilat formation were determined (Table 1), and representative Lineweaver-Burk plots are shown in Fig. 3, A–C. The K_i value of NDGA in HLM was 30-fold higher than that in RLM, suggesting species differences. The K_i value of NDGA in RLM was also much lower than that in RJM. Likewise, NDGA in RLC showed a lower K_i value than that in RJC. The inhibitory potency of
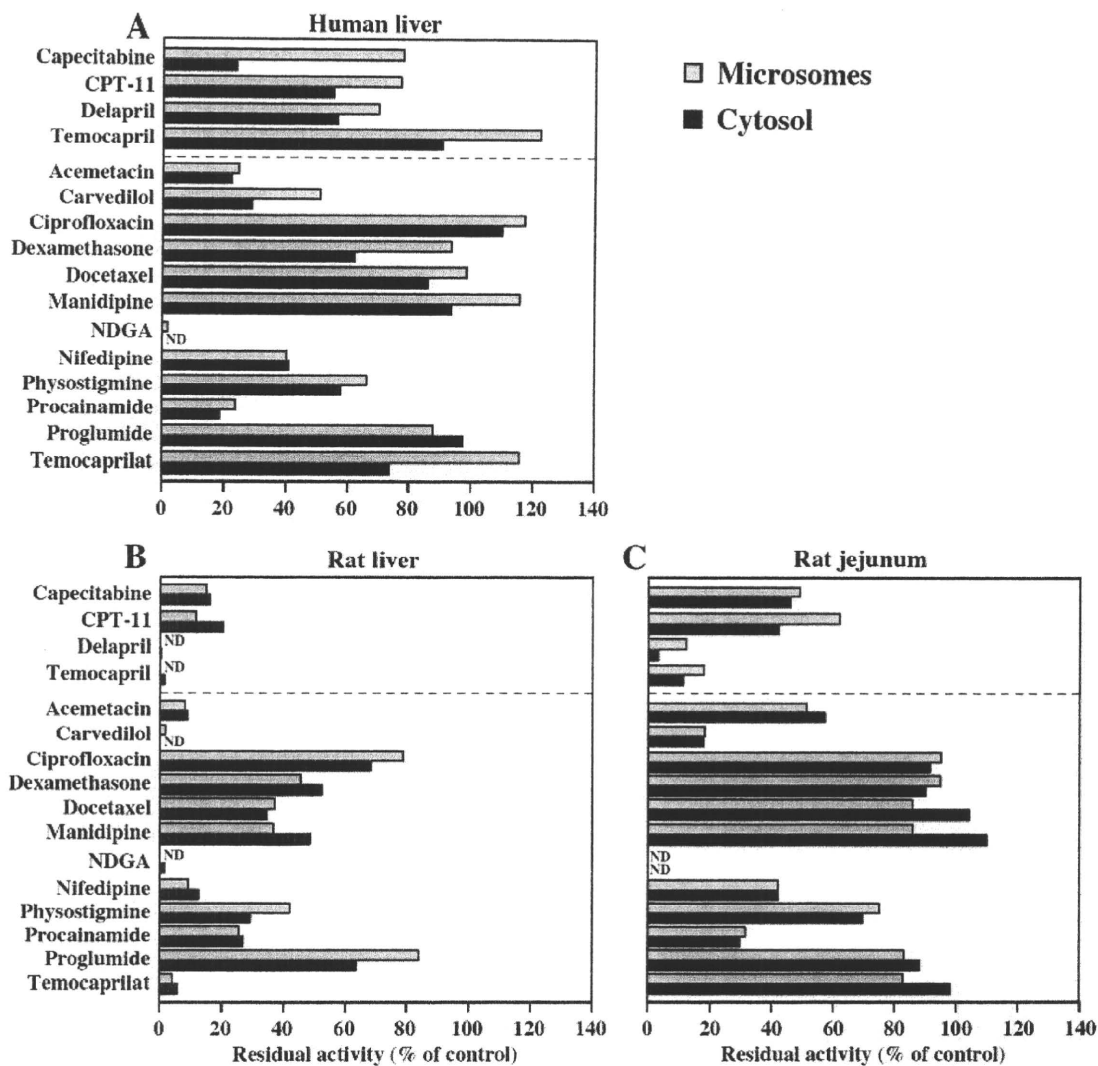
FIG. 1. Inhibitory effect of 15 drugs and 1 compound on imidaprilat formation catalyzed by HLM and HLC (A), RLM and RLC (B), and RJM and RJC (C). The concentrations of imidapril and the 15 drugs and 1 compound were 150 and 300 μM except for manidipine (50 μM), respectively. Each column represents the mean of duplicate determinations. The control activity was 0.4 nmol/min/mg protein in HLM, 0.05 nmol/min/mg protein in HLC, 37.6 nmol/min/mg protein in RLM, 17.6 nmol/min/mg protein in RLC, 0.8 nmol/min/mg protein in RJM, and 0.4 nmol/min/mg protein in RJC. ND, not detected.

procainamide in HLM was similar to that in HLC. The K_i value of carvedilol in RJM was approximately 5-fold higher than that in RLM. Compared with microsomes and cytosol from rat liver or jejunum, the K_i values of carvedilol were approximately 2-fold different.

Inhibition Constant and Inhibitory Patterns of SN-38 Formation. The K_i values and inhibition patterns for SN-38 formation were determined as shown in Table 2 and representative Lineweaver-Burk plots are shown in Fig. 3, D–F. The K_i values in RLM and RLC were not determined because the activity was not inhibited potently by any drugs or compound. The K_i value of carvedilol in HLM was lower than that in HLC. The K_i value of physostigmine in HJM was similar to that in RJM. On the other hand, the K_i value of physostigmine in HJC was 10-fold lower than that in RJC or HJM. The inhibitory potency of physostigmine in HLM was stronger than that in HJM. The K_i value of manidipine in HJC was lower than that in RJM or RJC.

Discussion

In multiple drug therapy, drug interactions are important issues that must be taken into consideration. It is possible that coadministration of several drugs can change the efficacy of a drug due to the inhibition of drug-metabolizing enzymes. Investigations of inhibitory effects for CES activity provide useful information for the prediction of in vivo drug interactions and for drug development. In the present study, we investigated the inhibitory effects on hydrolysis of two prodrugs in human and rat to clarify the species differences in CES inhibition. Imidapril and CPT-11 were used as representative CES1 and CES2 substrates.

In imidaprilat formation from imidapril by CES1, delapril and temocapril were inhibited weakly (>50% of control) in human liver, whereas they showed more than 90% inhibition in rat liver (Fig. 1). Human CES1 was shown to be less efficient at catalysis of bulky substrates than rabbit CES because of the size-limited access of substrates to the active site (Wadkins et al., 2001). Because delapril and temocapril are substrates of human CES1 (Takai et al., 1997) and are more bulky than imidapril, size differences of the active site between human and rat may have contributed to the present results.

Dexamethasone and docetaxel, which are not CES substrates, inhibited the imidaprilat formation weakly in human liver (Fig. 1). The
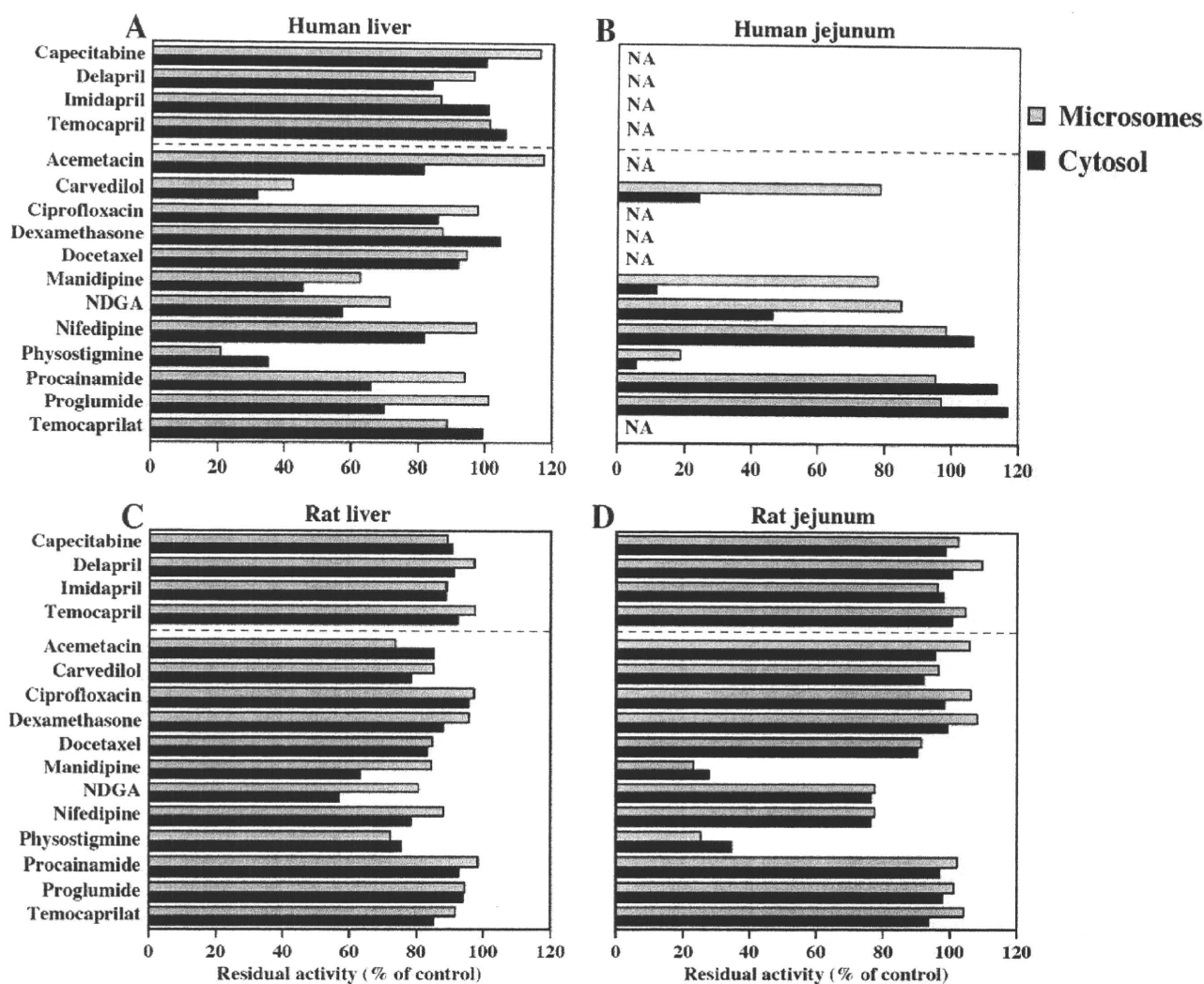
FIG. 2. Inhibitory effect of 15 drugs and 1 compound on SN-38 formation catalyzed by HLM and HLC (A), HJM and HJC (B), RLM and RLC (C), and RJM and RJC (D). The concentrations of CPT-11 and the 15 drugs and 1 compound were 5 and 10 μM, respectively. Each column represents the mean of duplicate determinations. The control activity was 3.7 pmol/min/mg protein in HLM, 0.9 pmol/min/mg protein in HLC, 0.6 pmol/min/mg protein in HJM, 6.5 pmol/min/mg protein in HJC, 5.1 pmol/min/mg protein in RLM, 2.3 pmol/min/mg protein in RLC, 13.5 pmol/min/mg protein in RJM, and 4.6 pmol/min/mg protein in RJC. NA, not available.

TABLE 1

K_i values and inhibition types for the imidaprilat formation

Data generated by nonlinear regression analysis are expressed as mean ± S.E. The concentrations of imidapril ranged from 100 to 500 μM for HLM and HLC, from 25 to 150 μM for RLM, from 15 to 90 μM for RLC, from 20 to 80 μM for RJM, and from 25 to 100 μM for RJC. The concentrations of inhibitors ranged as follows: for carvedilol, 1 to 6 μM for RLM, 1 to 6 μM for RLC, 4 to 24 μM for RJM, and 5 to 30 μM for RJC; for NDGA, 10 to 40 μM for HLM, 2 to 7 μM for HLC, 0.2 to 2 μM for RLM, 0.2 to 1.5 μM for RLC, 3 to 15 μM for RJM, and 2 to 12 μM for RJC; and for procainamide, 25 to 150 μM for HLM and 25 to 100 μM for HLC.

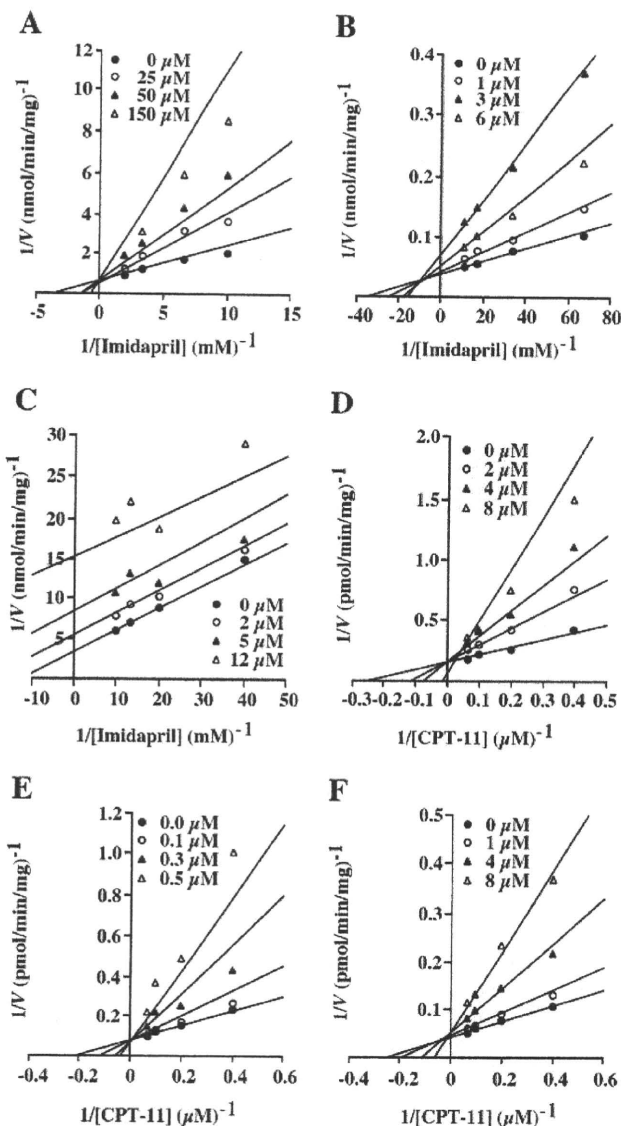| Enzyme Source	Inhibitor	K_i	Inhibition Type
		μM	
HLM	NDGA	13.3 ± 1.5	Mixed
	Procainamide	29.3 ± 4.8	Competitive
HLC	NDGA	2.9 ± 0.5	Uncompetitive
	Procainamide	34.5 ± 2.2	Competitive
RLM	Carvedilol	1.6 ± 0.2	Competitive
	NDGA	0.4 ± 0.0	Uncompetitive
RLC	Carvedilol	2.3 ± 0.3	Mixed
	NDGA	0.4 ± 0.0	Uncompetitive
RJM	Carvedilol	8.8 ± 0.5	Competitive
	NDGA	11.0 ± 2.2	Mixed
RJC	Carvedilol	5.1 ± 1.0	Competitive
	NDGA	3.2 ± 0.3	Uncompetitive

FIG. 3. Inhibitory effect of imidaprilat formation by procainamide (A), carvedilol (B), and NDGA (C) and SN-38 formation by carvedilol (D), manidipine (E), and physostigmine (F). A and D, HLM; B, RLC; C, RJC; E, HJC; F, RJM. Each point represents the mean of duplicate determinations. The control activity was the same as that in Figs. 1 and 2.

uncompetitive inhibition except for RJM, suggesting that NDGA could bind to a site different from the active site. In fact, human CES1 has ligand binding sites other than the active site, and each site is called a side door and a Z-site (Bencharit et al., 2003b). Rat CES isoforms may contain other sites such as human CES1. The inhibitory potencies of carvedilol were stronger in rat liver and jejunum than those in human liver (Table 1). Although the structures of rat CES isoforms have not been revealed, structural differences between human and rat CES may be involved in the species differences of the inhibition potency.

The inhibitory effects in both microsomes and cytosol showed similar tendencies in imidaprilat formations in human and rat in the present study. The activities in microsomes were more than 2-fold higher than those in cytosol. However, because the expression levels of cytosolic proteins are approximately 5-fold higher than those of microsomal proteins, the contribution of cytosolic CES is as important as that of microsomal CES (Tabata et al., 2004). Thus, CES inhibition in the cytosol as well as in microsomes should be taken into consideration.

SN-38 formations in jejunum were inhibited more strongly by manidipine than those in liver in the present study. Manidipine is similar in structure to nifedipine and has larger alcohol groups that are hydrolyzed well by CES2. Because nifedipine did not inhibit SN-38 formation in HJC, manidipine could be a potent CES2 inhibitor in human jejunum. Carvedilol also showed inhibitions for the SN-38 formations in both human liver and jejunum except HJM, whereas there were no inhibitions in rat liver and jejunum, indicating species differences in CES2 activity. As shown in Figs. 1 and 2, the SN-38 formations in all enzyme sources were not inhibited by procainamide, whereas the imidaprilat formations were inhibited strongly. The major isoforms involved in the hydrolysis of CPT-11 and imidapril are CES2 and CES1, respectively (Schwer et al., 1997; Takai et al., 1997). Human CES1 is also expressed in liver at much higher levels than in small intestine (Imai, 2006), whereas CES2 is abundant in small intestine (Schwer et al., 1997). Thus, procainamide exhibited more potent inhibitory effects for CES1 than for CES2.

Because there were no drugs and compounds that inhibited the SN-38 formations potently in rat liver, the K_i values in RLM and RLC were not determined. On the other hand, the SN-38 formations in RJM and RJC were inhibited competitively by manidipine with low K_i values, suggesting that tissue differences would exist in the inhibition of CPT-11 hydrolase activity. Satoh et al. (1994) demonstrated that ES-4 and ES-10 purified from RLM, which both belong to CES1 family, have the ability to hydrolyze CPT-11 more effectively than human CES1. By Northern blot analysis, both CES1 and CES2 were expressed in rat liver (Sanghani et al., 2002), whereas CES2 isoforms were mainly expressed in Wistar rat jejunum, but the mRNA expression levels of the CES1 isoforms were much lower than those of CES2 (Masaki et al., 2007). From these studies, it could be speculated that CES2 isoforms are responsible for CPT-11 hydrolysis; thus, the potent inhibitory effects by manidipine may be the result of CES2 inhibition in rat jejunum. Although the clinical serum concentration of manidipine is on the order of nanomolar concentrations, intestinal mucosa may be exposed to high concentrations of a given drug. Therefore, we have to keep the CES2 inhibition in mind in clinical practice. Manidipine also exhibited a potent competitive inhibition in HJC, whereas imidaprilat formations in human liver were not inhibited. The entrance to the active site of human CES1 is smaller than that for CES2 (Wadkins et al., 2001), leading to the difference in inhibition. Although the crystal structure of human CES2 is not obvious, human CES2 contains N-glycosylation sites at two positions, whereas CES1 has one N-glycosylation site (Bencharit et al., 2003a).

two drugs exhibited weak inhibitions for the hydrolysis of 4-methylumbelliferyl acetate catalyzed by both CES1A1 and CES2 (IC_{50} >0.7 mM) (Quinney et al., 2005), consistent with our results. As shown in Table 1, imidaprilat formation in HLM was inhibited competitively by procainamide. Bailey and Briggs (2003) suggested that procainamide inhibits human CES1. Procainamide is also known as a choline binding pocket-specific inhibitor (Jaganathan and Boopathy, 1998) and has been reported to inhibit human butyrylcholinesterase competitively ($K_i = 9$ μM) (Rush et al., 1981). Because the amino acid sequences at the active site were highly conserved among esterase B, which is inhibited by organophosphorus compounds such as CES and butyrylcholinesterase (Satoh and Hosokawa, 1995), it is reasonable to assume that procainamide inhibits CES1 activity. Imidaprilat formations in rat liver were inhibited more strongly by NDGA than those in human liver (Table 1). NDGA is known as a potent CES inhibitor (Schegg and Welch, 1984). These inhibition patterns showed

TABLE 2

K_i values and inhibition types for SN-38 formation

Data generated by nonlinear regression analysis are expressed as mean ± S.E. The concentrations of CPT-11 ranged from 2.5 to 15 μM for all enzyme sources. The concentrations of the inhibitors ranged as follows: for carvedilol, 2 to 8 μM for HLM and 1 to 12 μM for HLC; for manidipine, 0.1 to 0.5 μM for HJC, 0.5 to 5 μM for RJM, and 0.5 to 4 μM for RJC; and for physostigmine, 0.1 to 0.6 μM for HLM, 0.2 to 5 μM for HLC, 1 to 6 μM for HJM, 0.2 to 1 μM for HJC, 1 to 8 μM for RJM, and 2 to 10 μM for RJC.

Enzyme Source	Inhibitor	K_i	Inhibition Type
		μM	
HLM	Carvedilol	1.6 ± 0.2	Competitive
	Physostigmine	0.2 ± 0.0	Competitive
HLC	Carvedilol	4.1 ± 0.3	Competitive
	Physostigmine	1.6 ± 0.3	Competitive
HJM	Physostigmine	3.1 ± 0.2	Noncompetitive
HJC	Manidipine	0.1 ± 0.0	Competitive
	Physostigmine	0.3 ± 0.0	Mixed
RJM	Manidipine	0.8 ± 0.1	Competitive
	Physostigmine	2.5 ± 0.3	Mixed
RJC	Manidipine	0.6 ± 0.1	Competitive
	Physostigmine	3.1 ± 0.4	Mixed

In the present study, the K_i values of physostigmine, a specific cholinesterase inhibitor, were approximately 10-fold lower in HLM ($K_i = 0.2 \pm 0.0$ μM) and HJC ($K_i = 0.3 \pm 0.0$ μM) than the other enzyme sources. These K_i values were close to the previous result showing that physostigmine inhibited the hydrolysis of 4-methylumbelliferyl acetate by purified human CES2 ($K_i = 0.10 \pm 0.01$ μM) (Pindel et al., 1997). The CES1 and CES2 family share 40 to 50% amino acid sequence identity, but the substrate specificities of CES1 and CES2 in human are different; CES1 hydrolyzes compounds with larger acyl groups and CES2 preferentially hydrolyzes large alcohol groups (Satoh et al., 2002; Imai, 2006).

The present comprehensive study clarified that species differences existed in the inhibition of imidapril and CPT-11 hydrolysis and should provide useful information on the differences in CES activity in human and rat.

References

Bailey DN and Briggs JR (2003) Procainamide and quinidine inhibition of the human hepatic degradation of meperidine in vitro. *J Anal Toxicol* 27:142–144.

Bencharit S, Morton CL, Hyatt JL, Kuhn P, Danks MK, Potter PM, and Redinbo MR (2003a) Crystal structure of human carboxylesterase 1 complexed with the Alzheimer's drug tacrine: from binding promiscuity to selective inhibition. *Chem Biol* 10:341–349.

Bencharit S, Morton CL, Xue Y, Potter PM, and Redinbo MR (2003b) Structural basis of heroin and cocaine metabolism by a promiscuous human drug-processing enzyme. *Nat Struct Biol* 10:349–356.

Buratti FM and Testai E (2005) Malathion detoxification by human hepatic carboxylesterases and its inhibition by isomalathion and other pesticides. *J Biochem Mol Toxicol* 19:406–414.

Emoto C, Yamazaki H, Iketaki H, Yamasaki S, Satoh T, Shimizu R, Suzuki S, Shimada N, Nakajima M, and Yokoi T (2001) Cooperativity of α-naphthoflavone in cytochrome P450 3A-dependent drug oxidation activities in hepatic and intestinal microsomes from mouse and human. *Xenobiotica* 31:265–275.

Fleming CD, Bencharit S, Edwards CC, Hyatt JL, Tsurkan L, Bai F, Fraga C, Morton CL, Howard-Williams EL, Potter PM, et al. (2005) Structural insights into drug processing by human carboxylesterase 1: tamoxifen, mevastatin, and inhibition by benzil. *J Mol Biol* 352:165–177.

Humerickhouse R, Lohrbach K, Li L, Bosron WF, and Dolan ME (2000) Characterization of CPT-11 hydrolysis by human liver carboxylesterase isoforms hCE-1 and hCE-2. *Cancer Res* 60:1189–1192.

Imai T (2006) Human carboxylesterase isozymes: catalytic properties and rational drug design. *Drug Metab Pharmacokinet* 21:173–185.

Jaganathan L and Boopathy R (1998) Interaction of Triton X-100 with acyl pocket of butyrylcholinesterase: effect on esterase activity and inhibitor sensitivity of the enzyme. *Indian J Biochem Biophys* 35:142–147.

Linke T, Dawson H, and Harrison EH (2005) Isolation and characterization of a microsomal acid retinyl ester hydrolase. *J Biol Chem* 280:23287–23294.

Masaki K, Hashimoto M, and Imai T (2007) Intestinal first-pass metabolism via carboxylesterase in rat jejunum and ileum. *Drug Metab Dispos* 35:1089–1095.

Mésange F, Sebbar M, Capdevielle J, Guillemot JC, Ferrara P, Bayard F, Poirot M, and Faye JC (2002) Identification of two tamoxifen target proteins by photolabeling with 4-(2-morpholinoethoxy)benzophenone. *Bioconjug Chem* 13:766–772.

Murakami K, Takagi Y, Mihara K, and Omura T (1993) An isozyme of microsomal carboxyesterases, carboxyesterase Sec, is secreted from rat liver into the blood. *J Biochem* 113:61–66.

Pindel EV, Kedishvili NY, Abraham TL, Brzezinski MR, Zhang J, Dean RA, and Bosron WF (1997) Purification and cloning of a broad substrate specificity human liver carboxylesterase that catalyzes the hydrolysis of cocaine and heroin. *J Biol Chem* 272:14769–14775.

Quinney SK, Sanghani SP, Davis WI, Hurley TD, Sun Z, Murry DJ, and Bosron WF (2005) Hydrolysis of capecitabine to 5'-deoxy-5-fluorocytidine by human carboxylesterases and inhibition by loperamide. *J Pharmacol Exp Ther* 313:1011–1016.

Rush RS, Main AR, Kilpatrick BF, and Faulkner GD (1981) Inhibition of two monomeric butyrylcholinesterases from rabbit liver by chlorpromazine and other drugs. *J Pharmacol Exp Ther* 216:586–591.

Sanghani SP, Davis WI, Dumaual NG, Mahrenholz A, and Bosron WF (2002) Identification of microsomal rat liver carboxylesterases and their activity with retinyl palmitate. *Eur J Biochem* 269:4387–4398.

Sanghani SP, Quinney SK, Fredenburg TB, Davis WI, Murry DJ, and Bosron WF (2004) Hydrolysis of irinotecan and its oxidative metabolites, 7-ethyl-10-[4-N-(5-aminopentanoic acid)-1-piperidino] carbonyloxycamptothecin and 7-ethyl-10-[4-(1-piperidino)-1-amino]-carbonyloxycamptothecin, by human carboxylesterases CES1A1, CES2, and a newly expressed carboxylesterase isoenzyme, CES3. *Drug Metab Dispos* 32:505–511.

Satoh T and Hosokawa M (1995) Molecular aspects of carboxylesterase isoforms in comparison with other esterases. *Toxicol Lett* 82–83:439–445.

Satoh T, Hosokawa M, Atsumi R, Suzuki W, Hakusui H, and Nagai E (1994) Metabolic activation of CPT-11, 7-ethyl-10-[4-(1-piperidino)-1-piperidino]carbonyloxycamptothecin, a novel antitumor agent, by carboxylesterase. *Biol Pharm Bull* 17:662–664.

Satoh T, Taylor P, Bosron WF, Sanghani SP, Hosokawa M, and La Du BN (2002) Current progress on esterases: from molecular structure to function. *Drug Metab Dispos* 30:488–493.

Schegg KM and Welch W Jr (1984) The effect of nordihydroguaiaretic acid and related lignans on formyltetrahydrofolate synthetase and carboxylesterase. *Biochim Biophys Acta* 788:167–180.

Schwer H, Langmann T, Daig R, Becker A, Aslanidis C, and Schmitz G (1997) Molecular cloning and characterization of a novel putative carboxylesterase, present in human intestine and liver. *Biochem Biophys Res Commun* 233:117–120.

Tabata T, Katoh M, Tokudome S, Nakajima M, and Yokoi T (2004) Identification of the cytosolic carboxylesterase catalyzing the 5'-deoxy-5-fluorocytidine formation from capecitabine in human liver. *Drug Metab Dispos* 32:1103–1110.

Takahashi S, Katoh M, Saitoh T, Nakajima M, and Yokoi T (2008) Allosteric kinetics of human carboxylesterase 1: species differences and interindividual variability. *J Pharm Sci* 97:5434–5445.

Takai S, Matsuda A, Usami Y, Adachi T, Sugiyama T, Katagiri Y, Tatematsu M, and Hirano K (1997) Hydrolytic profile for ester- or amide-linkage by carboxylesterases pI 5.3 and 4.5 from human liver. *Biol Pharm Bull* 20:869–873.

Wadkins RM, Hyatt JL, Edwards CC, Tsurkan L, Redinbo MR, Wheelock CE, Jones PD, Hammock BD, and Potter PM (2007) Analysis of mammalian carboxylesterase inhibition by trifluoromethylketone-containing compounds. *Mol Pharmacol* 71:713–723.

Wadkins RM, Morton CL, Weeks JK, Oliver L, Wierdl M, Danks MK, and Potter PM (2001) Structural constraints affect the metabolism of 7-ethyl-10-[4-(1-piperidino)-1-piperidino]carbonyloxycamptothecin (CPT-11) by carboxylesterases. *Mol Pharmacol* 60:355–362.

Address correspondence to: Dr. Tsuyoshi Yokoi, Drug Metabolism and Toxicology, Faculty of Pharmaceutical Sciences, Kanazawa University, Kakumamachi, Kanazawa 920-1192, Japan. E-mail: tyokoi@kenroku.kanazawa-u.ac.jp

MicroRNA regulates human vitamin D receptor

Takuya Mohri, Miki Nakajima, Shingo Takagi, Sayaka Komagata and Tsuyoshi Yokoi*

Drug Metabolism and Toxicology, Faculty of Pharmaceutical Sciences, Kanazawa University, Kakuma-machi, Kanazawa, Japan

Most of the biological effects of 1α,25-dihydroxyvitamin D_3 (1,25$(OH)_2D_3$) are elicited by the binding to vitamin D receptor (VDR), which regulates gene expression. Earlier studies reported no correlation between the VDR protein and mRNA levels, suggesting the involvement of posttranscriptional regulation. MicroRNAs (miRNAs) are small noncoding RNAs that regulate gene expression through translational repression or mRNA degradation. A potential miR-125b recognition element (MRE125b) was identified in the 3′-untranslated region of human VDR mRNA. We investigated whether VDR is regulated by miR-125b. In luciferase assays using a plasmid containing the MRE125b, the antisense oligonucleotide for miR-125b significantly increased (130% of control) the reporter activity in KGN cells, whereas the precursor for miR-125b significantly decreased (40% of control) the reporter activity in MCF-7 cells, suggesting that miR-125b functionally recognized the MRE125b. By electrophoretic mobility shift assays, it was demonstrated that the overexpression of miR-125b significantly decreased the endogenous VDR protein level in MCF-7 cells to 40% of control. 1,25$(OH)_2D_3$ drastically induced the CYP24 mRNA level in MCF-7 cells, but the induction was markedly attenuated by the overexpression of miR-125b. In addition, the antiproliferative effects of 1,25$(OH)_2D_3$ in MCF-7 cells were significantly abolished by the overexpression of miR-125b. These results suggest that the endogenous VDR level was repressed by miR-125b. In conclusion, we found that miR-125b posttranscriptionally regulated human VDR. Since the miR-125b level is known to be downregulated in cancer, such a decrease may result in the upregulation of VDR in cancer and augmentation of the antitumor effects of 1,25$(OH)_2D_3$.
© 2009 UICC

1α,25-Dihydroxyvitamin D_3 (1,25$(OH)_2D_3$ or calcitriol), a biologically active metabolite of vitamin D_3, is known as a classical regulator of calcium and bone homeostasis.[1,2] Vitamin D deficiency is linked to rickets and osteoporosis.[3] Over the last 25 years, additional roles have been found for vitamin D in the regulation of cell processes such as cell growth, differentiation and apoptosis. Accumulating evidence has revealed that vitamin D deficiency is also associated with the risk of cancer.[4] Since the vitamin D system has relevance for both the prevention and treatment of cancer,[3] the development of a number of novel synthetic vitamin D analogues as a therapeutic agent in cancer has been attempted.

Most of the biological effects of 1,25$(OH)_2D_3$ are elicited by the binding to vitamin D receptor (VDR; NR1I1),[5] which belongs to the superfamily of nuclear steroid hormone receptors. After ligand binding, the VDR forms a heterodimer with retinoid X receptor (RXR; NR2B1) and binds to vitamin D responsive element (VDRE) in the regulatory region of the target genes.[6] The VDR is expressed not only in the classical vitamin D responsive organs including the intestine, bone and kidney but also in many other nonclassical vitamin D responsive organs including the liver, suggesting a broader role of the receptor.[7] It has been reported that, at the protein level, the VDR expression is higher in breast[8] and thyroid[9] cancers than in normal tissues, but no obvious difference was found in cancer and normal tissues at the mRNA level. In colon cancer, the VDR mRNA and protein expression levels are gradually increased in the early stages of cancerogenesis, but the VDR mRNA decreases subsequently to lower levels during advancement.[10] Thus, the VDR expression is upregulated in cancers, although the expression levels seem to change during disease progression and in response to therapies. However, the mechanism of the upregulation of VDR protein in cancer has not been clarified. One clue is that there is no correlation between the VDR protein and mRNA levels, suggesting the involvement of posttranscriptional regulation.

To uncover the molecular mechanism of the posttranscriptional regulation, we sought to determine whether microRNA (miRNA) might be involved in the regulation of VDR. MiRNAs are an evolutionarily conserved class of endogenous ∼22-nucleotide noncoding RNAs, and play a key role in diverse biological processes, including development, cell proliferation, differentiation, apoptosis and cancer initiation and progression.[11–13] MiRNAs recognize the 3′-untranslated region (3′-UTR) of the target mRNA and cause translational repression or mRNA degradation.[14] To date, ∼700 miRNAs have been identified in human, and more than one-third of all human genes have been predicted to be miRNA targets.[15] The expression of global miRNAs is deregulated in most types of human cancers.[13] In this study, we investigated the potential involvement of miRNAs in the posttranscriptional regulation of human VDR expression.

Material and methods

Chemicals and reagents

1,25$(OH)_2D_3$ was purchased from Wako Pure Chemical Industries (Osaka, Japan). The pGL3-promoter vector, phRL-TK plasmid, pT7Blue T-Vector and a dual-luciferase reporter assay system were purchased from Promega (Madison, WI). LipofectAMINE2000 and LipofectAMINE RNAiMAX were from Invitrogen (Carlsbad, CA). Pre-miR miRNA Precursors for miR-125b-1 and negative control #2 were from Ambion (Austin, TX). Antisense LNA/DNA mixed oligonucleotides (AsO) for miR-125b (5′-TCACAAGTTAGGGTCTCAGGGA-3′, underlined letters are LNA) and for negative control (5′-AGAC TAGCGG-TATCTTAAACC-3′) were from Greiner Japan (Tokyo, Japan). All primers and oligonucleotides were commercially synthesized at Hokkaido System Sciences (Sapporo, Japan). Antibodies to VDR (C-20) and RXRα(D-20) were from Santa Cruz Biotechnology (Santa Cruz, CA). Restriction enzymes were from Takara (Shiga, Japan), TOYOBO (Osaka, Japan) and New England Biolabs (Beverly, MA). All other chemicals and solvents were of the highest grade commercially available.

Cells and culture conditions

The human breast adenocarcinoma cell lines MCF-7 and MDA-MB-435, the human colon carcinoma cell lines LS180 and the human embryonic kidney cell line HEK293 were obtained from the American Type Culture Collection (Rockville, MD). The

human ovarian granulosa-like tumor cell line KGN[16] and the human hepatoma cell line HepG2 were obtained from Riken Gene Bank (Tsukuba, Japan). MCF-7 cells and LS180 cells were cultured in Dulbecco's modified Eagle's medium (DMEM) (Nissui Pharmaceutical, Tokyo, Japan) supplemented with 0.1 mmol/L nonessential amino acid (Invitrogen) and 10% fetal bovine serum (FBS) (Invitrogen). MDA-MB-435 cells and HepG2 cells were cultured in DMEM supplemented with 10% FBS. HEK293 cells were cultured in DMEM supplemented with 4.5 g/L glucose, 10 mmol/L HEPES and 10% FBS. KGN cells were cultured in a 1:1 mixture of DMEM and Ham's F-12 medium (Nissui Pharmaceutical) supplemented with 10% FBS. These cells were maintained at 37°C under an atmosphere of 5% CO_2-95% air.

Real-time RT-PCR for mature miR-125b

For the quantification of mature miR-125b, polyadenylation and reverse transcription were performed using an NCode miRNA First-Strand cDNA Synthesis Kit (Invitrogen) according to the manufacturer's protocol. The forward primer for miR-125b was 5'-TCC CTG AGA CCC TAA CTT GTG A-3', and the reverse primer was the supplemented universal qPCR primer. The real-time PCR was performed using a Smart Cycler (Cepheid, Sunnyvale, CA) with Smart Cycler software (version 1.2b) as follows. After an initial denaturation at 95°C for 30 sec, the amplification was performed by denaturation at 95°C for 10 sec, annealing and extension at 60°C for 10 sec for 45 cycles.

Construction of reporter plasmids

To construct luciferase reporter plasmids, various target fragments were inserted into the *XbaI* site, downstream of the luciferase gene in the pGL3-promoter vector. The sequence from +1786 to +1813 in the human VDR mRNA (5'-CAG GAG AAA TGC ATC CAT TCC TCA GGG A-3') was termed the miR-125b recognition element (MRE125b). The region from +1748 to +1860 containing the MRE125b in the human VDR mRNA was amplified by PCR using the following primers adapted to the *XbaI* site: 5'-TTT TCT AGA CTG CCT AAG TGG CTG CTG AC-3' and 5'-TTT TCT AGA CGC TGG ACA AGC GGG GCC-3'. The PCR product was digested with *XbaI* and the 119-bp fragment was cloned into pGL3-promoter vector, resulting in single (pGL3/F1) and reverse single (pGL3/R1) insertions. The fragment containing 3 copies of the MRE125b, 5'-CTA G*AC AGG AGA AAT GCA TCC ATT CCT CAG GGA* CAG AG*C AGG AGA AAT GCA TCC ATT CCT CAG GGA* CAG AG*C AGG AGA AAT GCA TCC ATT CCT CAG GGA* CAG AGT-3' (MRE125b is italicized), was cloned into the pGL3-promoter vector (pGL3/3xMRE). The complementary sequence of 3 copies of the MRE125b was also cloned into the pGL3-promoter plasmid (pGL3/3xMRE-Rev). A fragment containing the perfect matching sequence with the mature miR-125b, 5'-CTA G*AT CAC AAG TTA GGG TCT CAG GGA* T-3' (the matching sequence of miR-125b is italicized), was cloned into the pGL3-promoter vector (pGL3/c-125b). The nucleotide sequences of the constructed plasmids were confirmed by DNA sequencing analyses.

Luciferase assay

Various luciferase reporter plasmids (pGL3) were transiently transfected with phRL-TK plasmid into MCF-7 and KGN cells. Briefly, the day before transfection, the cells were seeded into 24 well plates. After 24 hr, 450 ng of pGL3 plasmid, 50 ng of phRL-TK plasmid and the precursors for miR-125b or control were cotransfected into MCF-7 cells using LipofectAMINE 2000. For KGN cells, 450 ng of pGL3 plasmid, 50 ng of phRL-TK plasmid and the AsOs for miR-125b or control were cotransfected using LipofectAMINE 2000. After incubation for 48 hr, the cells were resuspended in passive lysis buffer and then the luciferase activity was measured with a luminometer (Wallac, Turku, Finland) using the dual-luciferase reporter assay system.

Transfection of precursor for miR-125b into MCF-7 cells and preparation of nuclear extract and total RNA

To investigate the effects of miR-125b on the expression level of VDR protein, 50 nM precursors for miR-125b or control were transfected into MCF-7 cells using LipofectAMINE RNAiMAX. After 72 hr, nuclear extract was prepared using NE-PER Nuclear and Cytoplasmic extraction reagents (Pierce, Rockford, IL) and total RNA was prepared using ISOGEN according to the manufacturer's protocols. The protein concentration in the nuclear extract was determined using Bradford protein assay reagent (Bio-Rad, Hercules, CA) with γ-globulin as a standard.

Electrophoretic mobility shift assays

Human VDR cDNA was amplified by PCR using cDNA from human normal kidney with the forward primer 5'-TCC TTC AGG GAT GGA GGC AAT GGC-3' and the reverse primer 5'-CTG TCC TAG TCA GGA GAT CTC ATT GCC-3'. The PCR fragment was cloned into the pT7Blue T-Vector. The nucleotide sequences of the constructed plasmids were confirmed by DNA sequencing analyses. Human RXRα expression vector (pGEM-3Z/hRXRα) was previously constructed.[17] Using these plasmids and the TNT T7 Quick Coupled Transcription/Translation System (Promega), human VDR and RXRα proteins were synthesized *in vitro*. The oligonucleotide containing VDRE, 5'-aag CAC ACC cgg TGA ACT ccg-3' (the hexamer half-sites are capitalized), was from the human *CYP24* promoter.[18] Double-stranded oligonucleotides were labeled with [γ-^{32}P]ATP using T4 polynucleotide kinase (TOYOBO) and purified by Microspin G-50 columns (GE Healthcare Bio-Sciences, Piscataway, NJ). The labeled probe (40 fmol, ~10,000 cpm) was applied to each binding reaction in 25 mM HEPES-KOH buffer (pH 7.9), 0.5 mM EDTA, 50 mM KCl, 10% glycerol, 0.5 mM dithiothreitol, 0.5 mM (*p*-amidinophenyl) methanesulfonyl fluoride, 2 μg of poly(dI-dC) and 2 μL of *in vitro* transcribed/translated proteins to a final reaction volume of 15 μL. For supershift experiments, 0.2 μg of anti-VDR antibodies or 2 μg of anti-RXRα antibodies were preincubated with *in vitro* transcribed/translated proteins or the nuclear extract at room temperature for 30 min. The mixtures were incubated on ice for 15 min and then loaded on 4% acrylamide gels in 0.5 × Tris-borate EDTA buffer. The gels were dried and then the DNA-protein complexes were detected with a Fuji Bio-Imaging Analyzer BAS 1000 (Fuji Film, Tokyo, Japan).

Real-time RT-PCR for CYP24

To investigate the effects of miR-125b on the induction of CYP24 mRNA by 1,25(OH)$_2$D$_3$, 50 nM precursors for miR-125b or control were transfected into MCF-7 cells using Lipofect-AMINE RNAiMAX. After 72 hr, the cells were treated with 100 nM 1,25(OH)$_2$D$_3$ (or 0.1% ethanol for control) for 24 hr. Total RNA was prepared using ISOGEN. The forward and reverse primers for CYP24 mRNA were 5'-CAG CAA ACA GTC TAA TGT GG-3' and 5'-AGC ATA TTC ACC CAG AAC TG-3', respectively. The real-time PCR analysis was performed as follows: after an initial denaturation at 95°C for 30 sec, the amplification was performed by denaturation at 94°C for 4 sec, annealing and extension at 62°C for 20 sec for 45 cycles. The CYP24 mRNA levels were normalized with GAPDH mRNA as described previously.[19]

Growth assay

To investigate the effects of miR-125b on the antiproliferative effects of 1,25(OH)$_2$D$_3$, growth assay was conducted according to the method by McGaffin *et al.*[20] with slight modifications. MCF-7 cells were plated on 96 well plates (3000 cells/well) and 20 nM precursors for miR-125b or control were transfected using LipofectAMINE RNAiMAX. After 24 hr, the cells were treated with 1 μM 1,25(OH)$_2$D$_3$ (or 0.1% ethanol) for 48–96 hr. The cells were rinsed with phosphate-buffered saline, fixed with 3.7% formaldehyde for 15 min and stained with 0.1% crystal violet for 10 min. The stained cells were washed with water and air dried. Crystal